Distributed rhythm generators underlie *Caenorhabditis elegans* forward locomotion

Anthony D. Fouad[1], Shelly Teng[1], Julian R. Mark[1], Alice Liu[1], Hongfei Ji[1], Eli Cornblath[1], Asuka Guan[2], Mei Zhen[2], and Christopher Fang-Yen[1]

1. Department of Bioengineering, School of Engineering and Applied Science, University of Pennsylvania, Philadelphia PA 19104, USA

2. Lunenfeld-Tanenbaum Research Institute, Mount Sinai Hospital, Toronto, Ontario M5G 1X5, Canada

Corresponding Author and Lead Contact: Christopher Fang-Yen, fangyen@seas.upenn.edu

ABSTRACT

Coordinated rhythmic movements are ubiquitous in animal locomotory, feeding, and circulatory systems. In many organisms, a chain of neural oscillators underlies the generation of rhythmic waves. In *C. elegans*, the nature of wave generation has been poorly understood; in particular, it has been unclear where in the locomotor circuit rhythm generation occurs, and whether there exists more than one such generator. We used targeted optogenetic manipulation and laser ablation experiments to probe the nature of rhythm generation in the locomotor circuit. We found that multiple sections of forward locomotor circuitry are capable of independently generating rhythms. By perturbing different components of the motor circuit, we localize the source of multiple secondary rhythm generators to cholinergic motor neurons in the midbody. Using rhythmic optogenetic perturbation we demonstrate a bidirectional entrainment between different sections of the body. These results show that like the vertebrate spinal cord, the *C. elegans* motor circuit contains multiple oscillators that normally coordinate their activity to generate behavior. Our work opens the possibility of a genetic and neural dissection of how rhythmic locomotion is generated, propagated, and modulated.

INTRODUCTION

Oscillatory neural activity underlies rhythmic animal behaviors including feeding and locomotion (Grillner, 2003). These oscillations are often generated by central pattern generators (CPGs), neuronal oscillators capable of generating rhythms in the absence of sensory feedback (Kiehn, 2006; Marder and Calabrese, 1996). CPGs can consist of single oscillator neurons, or networks of cells. The contribution of CPGs to animal locomotion has been studied in multiple vertebrate and invertebrate preparations. Isolated spinal cord preparations have been shown to produce fictive rhythmic and coordinated motor patterns (Kiehn, 2006).

The identification and study of locomotor CPGs in the mammalian spinal cord has been complicated by the vast numbers of neurons that are potentially involved (Kiehn, 2006). Small vertebrate and invertebrate model organisms with simpler circuitry have been an attractive and fruitful system in which to study the basic function of neural oscillators. For example, the identification of chains of CPGs in the leech and lamprey allowed models of locomotion to be constructed for these animals in greater detail than possible in more complex organisms (Marder et al., 2005). However, these studies have been limited by the paucity of genetic manipulations available in these organisms.

The microscopic roundworm *C. elegans* is a particularly promising model for an integrated circuit and molecular understanding of how locomotion is generated and coordinated. *C. elegans* has a compact nervous system containing 302 neurons, and is the only animal for which a nearly complete connectome, or wiring diagram of synaptic connectivity, has been mapped (Varshney et al., 2011; White et al., 1986). Worms' optical transparency allows researchers to monitor neural activity with calcium and voltage sensors (Flytzanis et al., 2014; Kerr, 2006; Kerr et al., 2000), and manipulate neurons and muscles using optogenetics (Husson

et al., 2012; Kocabas et al., 2012; Leifer et al., 2011; Stirman et al., 2011; Zhang et al., 2007). *C. elegans* is readily amenable to a powerful set of genetic manipulations (Ahringer, 2006; Evans, 2006). *C. elegans* shares extensive genetic homology with humans (Lai et al., 2000). Included among the shared machinery are a wide range of neurotransmitters, channels, and receptors (Altun and Hall, 2011; Gao et al., 2015; Pierce-Shimomura et al., 2008).

C. elegans moves forward by generating sinusoidal dorso-ventral bending waves that propagate from anterior to posterior. The circuit for locomotion consists of interneurons, excitatory and inhibitory motor neurons, and body wall muscles (Altun and Hall, 2011; Chalfie et al., 1985; White et al., 1986; White et al., 1976). Motor neuron cell bodies are located in the ventral nerve cord (VNC), which runs along the ventral side of the body from head to tail (Altun and Hall, 2011; White et al., 1986). The VNC motor neurons include A, B, VC, D, and AS type neurons. Laser ablation studies have shown that the A-type motor neurons are essential for reverse locomotion, whereas the B-type motor neurons are required for forward locomotion (Chalfie et al., 1985). The D-type (GABAergic) motor neurons are required for a normal amplitude of body bending waves but are not essential for locomotion itself (McIntire et al., 1993b). The function of the AS neurons is unknown. The VC neurons are involved in egg laying (Waggoner et al., 1998). These classes all form neuromuscular junctions with body wall muscles (BWMs).

While this basic architecture of the motor circuitry has been delineated by laser ablation studies, much less is understood about how its elements interact to generate coordinated locomotory behavior. For example, it is not known what elements generate the dorso-ventral oscillations during forward movement. Neither the identity nor the number of rhythm generators in the circuit are known. However, worms are able to generate local body bends despite ablation of most premotor interneurons (Chalfie et al., 1985; Kawano et al., 2011; Wicks and Rankin, 1995; Zheng et al., 1999; Kawano, Po, and Zhen, Personal Communication), and are capable of forward locomotion after ablation of all premotor interneurons and A motor neurons (Gao et al;

accompanying paper), suggesting that periodic bending may be organized at the level of the motor neurons or muscles.

Sensory feedback plays an important role in coordinating motor behavior. Experiments in which the worm's body was partially immobilized in a microfluidic device showed that the posterior B-type motor neurons mediate an anterior-to-posterior proprioceptive feedback mechanism (Wen et al., 2012). B-type motor neurons sense the body curvature and induce bending in the same direction (ventral or dorsal) posterior to the sensed bending. These results suggested a model, similar to one previously proposed (Karbowski et al., 2008), in which a single rhythmic generator generates bending oscillations in the head, and the remainder of the body propagates undulations from anterior to posterior via proprioceptive feedback (Wen et al., 2012). This model successfully reproduced the variation in locomotory characteristics in varied mechanical environments (Fang-Yen et al., 2010). This work demonstrated how a wave can be propagated along the body, but did not directly address the location and identity of the rhythmic generator(s). Furthermore, it focused on the posterior of the worm and did not determine whether head and neck proprioception is similarly essential for locomotion.

How might the locomotory circuit be organized? A single-oscillator model (**Figure 1C**) predicts that a disruption in body bending at any location will inhibit posterior bending (**Figure 1E**). Some alternative possibilities (Gjorgjieva et al., 2014; Zhen and Samuel, 2015) include the presence of multiple oscillators distributed along the motor circuit (**Figure 1D**), as there are in the vertebrate spinal cord (Kiehn, 2006). These oscillator units could be capable of generating undulations in the posterior of the worm even if neural activity or physical bending is interrupted anterior to their location (**Figure 1F**).

In this work, we used spatiotemporally targeted optogenetic illumination (Leifer et al., 2011; Stirman et al., 2011) and lesion studies to reveal that the mid-body VNC motor circuit contains

multiple units capable of independent oscillation. We found a fundamental architecture in the *C. elegans* motor circuit that bears striking resemblance to that of the mammalian spinal cord.

RESULTS

Rhythmic body bending in the worm posterior persists despite anterior paralysis

We first sought to test a model in which there is a single oscillator in the head and proprioceptive feedback is the dominant organizer of bending waves along most of the body (**Figure 1C**). This model, supported by experiments showing that immobilization of the mid-body of worms eliminated wave propagation posterior to the immobilized region (Wen et al., 2012), predicts that paralysis of any region will eliminate undulations posterior to the paralyzed region (**Figure 1E)**. In particular, we asked whether paralysis of the head and "neck" (a region immediately posterior to the head) would halt body bending posterior to these regions.

To manipulate neural and muscular activity in freely moving worms, we constructed an optogenetic targeting system similar to that previously described (Leifer et al., 2011). Briefly, this system uses real-time imaging processing algorithms and a digital micromirror device to project laser illumination onto arbitrarily specified regions of an unrestrained worm.

We used our system to illuminate worms expressing the inhibitory opsin halorhodopsin (NpHR/Halo) in all body wall muscles under the control of the *myo-3* promoter (Leifer et al., 2011; Zhang et al., 2007). We quantified the movement of worms before and during optogenetic manipulation by measuring the curvature of the worm centerline as a function of time and body coordinate (**Figure 1 A, B**) (Fang-Yen et al., 2010; Leifer et al., 2011; Pierce-Shimomura et al., 2008; Wen et al., 2012).

We specify longitudinal positions via a body coordinate ranging from 0 at the tip of the head to 100 at the end of the tail. Illuminating body coordinates 50-65 in P*myo-3::NpHR* worms caused near paralysis in the tail (not shown), consistent with previous findings (Leifer et al., 2011; Wen et al., 2012). When we paralyzed the anterior 33% or 45% of the worm, however, we observed robust oscillations in posterior regions of the body. In fact, illumination of the anterior 33% of the worm caused the tail's frequency to *increase* (**Figure 2A, C; Movie S1**).

Next, we asked whether the oscillations in the posterior would persist if the paralysis in the head and neck were mediated by optogenetic inhibition of excitatory motor neurons rather than muscles. We illuminated worms that express NpHR in all cholinergic neurons (P*unc-17::NpHR*), including the B-type motor neurons, head motor neurons, and several other types of neurons (Duerr et al., 2008). We found that optogenetic inhibition of cholinergic neurons in the head and neck caused head paralysis, but the tail undulation often persisted (**Figure 2B, C, Movie S1**).

During optogenetic muscle or neuron inactivation, the amplitude of the bending wave in the head decreased greatly but did not entirely vanish (**Figure 2A, B, D**), leaving open the possibility that a small amplitude residual wave propagates the bending wave through the partially paralyzed region. We therefore sought a more effective method to paralyze the head.

We found that touching a hot copper wire attached to a soldering iron to the anterior half of a worm rendered the treated part of the body almost completely immobile. After this treatment, rhythmic undulation routinely persisted in the tail even while the head and neck were nearly motionless (**Figure S1, Movie S1**).

The finding that posterior undulation can persist during partial or complete anterior paralysis is consistent with the multi-oscillator model (**Figure 1D**) and not consistent with a single oscillator model that relies on reflex-like signaling to propagate waves (**Figure 1C**).

The head and tail are capable of simultaneous oscillations at different frequencies

The finding that optogenetic inhibition of muscles in the animal's anterior induces higher frequency oscillations in the posterior suggests that an interruption of propagating activity in the motor circuit causes independent activity in a posterior oscillator. To test this idea further, we applied several optogenetic manipulations to inhibit motor coupling in the neck only, leaving the head and tail free to oscillate.

First, we optogenetically inhibited neck muscles in P*myo-3::NpHR* worms. In most trials, optogenetically inhibiting neck muscles prevented waves generated in the head from propagating through the neck. Absent new bending waves from the head, the tail exhibited a higher frequency bending wave, resulting in the animal simultaneously undulating at two distinct frequencies (**Figure 3A, Movie S2**). We henceforth refer to this phenomenon as two-frequency undulation (2FU).

We observed 2FU upon inhibiting the neck cholinergic neurons (**Figure 3B, Movie S2**) and also upon inhibiting neck B-type motor neurons (P*acr-5::Arch*; **Figure 3C, Movie S2**). These manipulations led to a large decrease in wave amplitude in the neck and a smaller decrease in wave amplitude in the tail (**Figure 3E**). Nevertheless, multiple animals in each experiment showed 2FU, with the highest ratios of tail frequency to head frequency seen in worms in which the neck muscles were inhibited (**Figure 3D**).

In many cases, the disruptions to coupling did not completely block wave transmission through the paralyzed region. Some waves that began in the head appeared to resume as if undisturbed in the tail, whereas other waves appeared to originate in the tail (**Figure 3C**). Nevertheless, the difference between head and tail frequencies during 2FU is inconsistent with a single oscillator model, rather, it suggests the existence of multiple units capable of independent oscillations.

If the posterior motor circuit contains additional oscillating units, we reasoned that localized undulations might occur after selectively activating small portions of the motor circuit while inhibiting all other portions. We therefore examined worms in which both the inhibitory opsin NpHR and the excitatory opsin channelrhodopsin-2 (ChR2) were expressed in the cholinergic neurons, after the A-type motor neurons were ablated by illumination of a photosensitizer fluorescent protein expressed in these cells (via the transgene P*unc-4::miniSOG*).

We first illuminated these animals with yellow light throughout the body to inhibit all cholinergic neurons, then targeted small portions of the tail with blue light, activating ChR2 and stimulating the most posterior B and AS neurons. Under these conditions, multiple animals generated very high frequency undulations in the tail (**Figure S2A, Movie S3**).

If multiple independent oscillators underlie a worm's forward movement, independent head and tail oscillations might also be observable in animals under more physiological conditions. Wave frequency depends strongly on the degree of mechanical loading from the environment, with frequency decreasing with viscosity of the medium (Fang-Yen et al., 2010). We hypothesized that head and tail oscillations may be decoupled by placing the anterior and posterior of a worm in fluids of different viscosities. When we studied worms transitioning between regions of a low viscosity buffer into highly viscoelastic hydroxypropylmethylcellulose (HPMC) islands (see Methods), we observed 2FUin 6 out of 41 worms (15%). In these animals, the tail continued oscillating at a high frequency for at least two full cycles even as the head frequency was sharply reduced (**Figure S2B, Movie S3**). Although these events were rare, they demonstrated that 2FU can occur in a wild type animal with no circuit perturbation.

These results strongly suggest that the *C. elegans* forward motor circuit contains at least two units capable of independent rhythm generation, and that a partial breakdown in anterior

proprioceptive coupling (by inhibiting neck BWMs) is sufficient to reveal the activity of the posterior oscillating unit(s).

Premotor interneurons are not essential for forward movement or 2FU

To better understand the source of tail oscillations during 2FU, we used genetic analysis and lesion studies to ask which components of the motor circuit are required for this behavior. Almost all chemical or electrical synaptic connections to the VNC motor neurons are made by the premotor interneuron (IN) classes AVB, PVC, AVA, AVD, and AVE (White et al., 1986). Laser ablation studies have indicated that AVB, and to a lesser degree PVC, are essential for normal forward locomotion (Chalfie et al., 1985). Therefore, we asked whether 2FU is possible in the absence of AVB, PVC and all other premotor INs.

To determine if the premotor interneurons are required for 2FU, we first asked whether optogenetic muscle inhibition in the neck in these worms lacking premotor interneurons would induce 2FU, as it does in worms with intact premotor neurons (**Figure 3A, D**). We first utilized transgenic strains in which expression of the apoptosis-promoting enzyme ICE was used to ablate premotor INs and some other neurons. When ICE is expressed under the control of the *nmr-1* or *glr-1* promoters, the PVC, AVA, AVD, and AVE interneurons are removed. AVB, however, are present in *Pnmr-1::ICE* worms, and may not be consistently ablated in P*glr-1::ICE* (Kawano et al., 2011; Kawano, Po, and Zhen, Personal Communication). We generated the strains P*myo-3::NpHR*; P*glr-1::ICE* and P*myo-3::NpHR*; P*nmr-1::ICE*. We found that both strains were capable of 2FU during optogenetic inhibition of neck muscles (**Figures 4A, E, S3A, D**). This result demonstrates that 2FU does not require most premotor interneurons, including the forward locomotory interneurons neurons PVC.

The interneuron AVB, unlike PVC, is coupled to the B-type motor neurons by an extensive network of gap junctions. Formation of these connections requires UNC-7 expression in AVB and UNC-9 expression in the B-type motor neurons (Starich et al., 2009). UNC-9 is also required for normal electrical coupling between BWM cells (Liu et al., 2006). We asked whether animals lacking UNC-7 or UNC-9 could exhibit 2FU during neck muscle paralysis. We crossed *unc-7* and *unc-9* mutations into our P*myo-3::NpHR* strain and performed optogenetic experiments as before. Because *unc-7* and *unc-9* worms were uncoordinated and could not sustain forward locomotion (Kawano et al., 2011; Starich et al., 2009), a mechanical stimulus in the form of a 3-5 s, ~200 Hz vibration of the slide using a cell phone motor was applied just before illumination to initiate a short bout of forward locomotion. We found that both strains were highly capable of 2FU (**Figures 4B, E**, **S3B, D**). This finding shows that gap junctions between AVB and the B-type motor neurons are not required for 2FU, further supporting the result that 2FU does not require the premotor interneurons.

Several classes of motor neurons are not required for forward locomotion or 2FU

The premotor interneurons comprise the primary circuit connection between the VNC motor neurons and the worm's other sensory and interneuron circuits (White et al., 1986). The finding that they are not required for forward locomotion and 2FU suggests that the source of high frequency tail undulations during 2FU may be the motor neurons themselves. We therefore asked whether any classes of motor neurons are required for 2FU during neck paralysis.

We first sought to determine whether the A-type motor neurons are required for 2FU. While the A class motor neurons are preferentially active during reverse locomotion (Haspel et al., 2010; Kawano et al., 2011), and are required for reverse locomotion (Chalfie et al., 1985), it is conceivable that they play a role in 2FU. We found that ablating the A- and VC-type motor

neurons with a genetically targeted ROS generator (P*unc-4::miniSOG*) did not prevent 2FU during forward locomotion (**Figure S3C, D**). This result supports the idea that the A and VC type motor neurons are not required for the posterior forward oscillator(s).

Next, we asked whether the GABAergic D-type motor neurons are required for 2FU. The D-type motor neurons release GABA onto the UNC-49 receptor to trigger contralateral muscle inhibition during a bend. Therefore, the putative null allele *unc-49(e407)* (Bamber et al., 1999; Liewald et al., 2008), should effectively block the functional output of D-type motor neurons. Indeed, *unc-49* mutants exhibited simultaneous dorsal and ventral contractions when stimulated for forward and reversal movement (McIntire et al., 1993a). We found that animals harboring an *unc-49(e407)* mutation, while very slow swimmers, were nonetheless capable of 2FU during neck muscle paralysis (**Figure 4D, E**).

The B-type motor neurons are required for forward locomotion (Chalfie et al., 1985; Wen et al., 2012), and are active during forward locomotion (Haspel et al., 2010; Kawano et al., 2011; Wen et al., 2012). However, we sought to determine whether any individual or small group of these neurons is essential for 2FU. To approach this question, we ablated groups of 2-6 B-type motor neurons at a time using a modified pulsed infrared laser system (Churgin et al., 2013; Methods). In all cases, at least some worms subject to each ablation were capable of 2FU (**Figures 4C, 4F, S4, S5**).

Taken together, these results suggest that no single neuron within the forward locomotor circuit is essential for generating high frequency tail rhythms during 2FU. The premotor interneurons, A, VC and D motor neurons are not required for 2FU. Our results are consistent with a model in which posterior rhythm generation can arise from multiple subsets of B or AS motor neurons.

Multiple segments of the tail are capable of independent rhythm generation

The observation that 2FU could persist despite disruptions to the various components of the mid-body motor circuitry suggested to us that one or more classes of neurons in the head are responsible for the observed high frequency tail undulations. Although we showed that the premotor INs are not required for 2FU, there are some connections between head neurons and the anterior VNC motor neurons that bypass the INs (White et al., 1986). To ascertain whether the mid-body motor circuit is capable of independent rhythm generation, we developed a method for eliminating synaptic connections between the mid-body motor neurons and the head circuits. We used our infrared laser system to cut both the VNC and the dorsal nerve cord (DNC) just posterior to the pharynx. In many cases, this procedure also severed other fasciculated process bundles that run parallel to the VNC and DNC (**Figure 5A**).

After disruption of the nerve cords, most animals were inactive (not shown), but could be induced to an active state by application of a mechanical stimulus. Nearly all of these worms could generate robust oscillations posterior to the cut location (**Figure 5A, E, Movie S4**). Moreover, the tail often undulated at a higher frequency than the mid-body (**Figure 5E**). In these worms, oscillations in the head were highly disrupted. In some cases, such as in Figure 5A, low amplitude waves propagating in the posterior-to-anterior direction occurred simultaneously with robust mid-body and tail waves propagating in the anterior-to-posterior direction. These results show that synaptic connections from the head circuits to the motor neurons are not required for wave generation posterior to the head.

It is possible that in this experiment, midbody undulations were being caused by small movements in the head rather than generated by a second oscillator. To exclude this possibility, we introduced an additional manipulation to reduce head movement. Using our infrared laser, we applied thermal damage to the worm's nerve ring (located in the head) in addition to cutting both nerve cords (see methods). Worms subjected to this procedure exhibited very little movement in the head. However, they continued to generate robust oscillations in the

midbody and even higher frequency oscillations in the tail (**Figure 5B, E, Movie S4**). The pattern of locomotion in thermally lesioned animals strongly resembled the 2FU induced by optogenetic perturbation, with the important difference that in our thermally lesioned animals, both frequencies were likely generated *outside* the head.

The emergence of multiple frequencies of undulation *outside* the head suggests that the VNC motor circuit itself may contain multiple units capable of independent oscillation. These units may exist in addition to any oscillating unit(s) in the head. To test this possibility directly, we next cut the VNC and DNC in two locations: in the neck (anterior to VB3) and in the tail (posterior to VB8). We again thermally lesioned the head neurons to suppress head movement. Under these conditions, the VNC motor neurons between VB3 and VB8 are isolated from circuitry in both the head and tail, and the VNC motor neurons posterior to VB8 are isolated from both the head circuits and the anterior VNC motor neurons. As before, these animals could generate robust body oscillations posterior to the first cut and higher frequency oscillations posterior to the second cut (**Figure 5C, E, Movie S4**), suggesting that rhythms can arise independently from each of these segments of the VNC motor neurons.

The A motor neurons were not required for 2FU (Figure S3C). We hypothesized that they are similarly not required for body oscillation after severing the nerve cords. We generated a strain expressing P*unc-17::GFP* and P*unc-4::miniSOG*, exposed the animals to blue light at the L2 stage to ablate A motor neurons, and again ablated the VNC and DNC in either one or two locations. Animals in which the VNC and DNC had been severed near the head were capable of robust wave generation and propagation posterior to the head (Figure S6B). Animals in which the VNC and DNC were severed in two locations were capable of rhythmic activity in the mid-body or tail, although we did not observe any cases of simultaneous oscillation in each segment (N=20 worms, Figure S6C). These results support the idea that the A motor neurons are not required for oscillation in surgically isolated segments of the VNC motor circuit.

The observation that anterior VNC/DNC cuts disrupt normal head undulation (**Figure 5A**) suggests that the head circuits are incapable of rhythm generation without input from the VNC. To address this possibility, we studied additional worms in which the VNC/DNC were cut in 2 locations, but which were not subject to thermal damage to the head. As in our earlier experiment (Figure 5A), head movement was highly disrupted (not shown). However, we occasionally observed very slow head undulation in these animals, indicating that head undulation is still possible under these conditions (**Figure 5D**, **Movie S4**).

Taken together, these results suggest that the *C. elegans* forward locomotor circuitry possesses at least three units capable of independent oscillation, with two units located outside the head. Although we did not observe simultaneous 3-frequency forward undulation in any animal tested, we have shown that oscillations are possible in each segment after completely severing motor inputs from all other segments. Lastly, these results confirm the idea that input from the premotor interneurons is not required for rhythm generation in the mid-body (c.f. Figure 4), as both AVB and PVC send their processes through the ventral nerve cord. The mid-body undulations observed after cutting the nerve cords both anterior and posterior to the source (**Figure 5C**) provide evidence that the VNC motor neurons are capable of rhythm generation.

Undulations can arise in arbitrary portions of the VNC motor circuit

We next sought to identify the smallest portion of the VNC motor circuit that is capable of generating rhythmic behaviors, and whether any differences exist between the rhythmic properties of segments of various sizes. To address these questions, we again severed the VNC and DNC in one location and damaged the head (as in Figure 5B), but we systematically varied the location of the VNC/DNC lesions relative to the B motor neurons.

When we severed the VNC and DNC at arbitrary locations (anterior to VB3, VB5, VB6, VB7, VB9, VB10, and VB11), we found that undulations posterior to the damage began near each cut location (**Figure 6B-E**). Bending amplitude similarly recovered just posterior to each cut location, rather than at a fixed body coordinate (**Figure 6F**). Interestingly, oscillations in the tail usually occurred at a higher frequency when the nerve cords were severed in the tail than when they were severed near the head (**Figure 6G**). We did not observe any bouts of locomotion with anterior-to-posterior waves posterior to the lesions when we severed the nerve cords anterior to VB11 (not shown), and bouts detected after lesioning at VB10 had waves of very low amplitude (Figure 6F) and somewhat ambiguous rhythmicity (not shown). The smallest VNC segment that produced clear and robust rhythmic waves was the region between VB9 and the tail.

These results suggest that the most compact rhythm-generating unit of the forward motor circuit is at least as small as the region containing VB9, VB10, VB11, DB6, and DB7.

Rhythmic motor entrainment is possible in both the anterior and posterior directions

Although we have shown that the *C. elegans* forward motor circuitry contains multiple rhythm generating units, it remains unclear exactly how these oscillators are coupled together, or even if they are all active during normal locomotion. Previous work has demonstrated proprioceptive coupling in the posterior direction (Wen et al., 2012), and we showed that a disruption to proprioceptive coupling (via optogenetic inhibition of neck muscles) could be used to decouple body undulations from head movements (**Figures 3A, 4**). However, one surprising feature of our results was that paralyzing the neck muscles appeared to decrease the head frequency. We found that during 2FU, head frequency significantly decreases and tail frequency significantly increases relative to the natural swimming frequency (**Figure 7A**). This observation suggests

that anteriorward coupling, in addition to posteriorward coupling, may be present in the forward movement circuitry.

To test for anteriorward coupling between motor circuit elements, we asked whether an oscillating optogenetic perturbation in the mid-body can entrain the head to a new frequency. We used our optogenetic targeting system to rhythmically inhibit the mid-body BWMs (**Figure 7B**). Worms subject to this procedure exhibit a head bending frequency approximately one half that of the imposed frequency. The factor of one half is likely due to the presence of two phases during the rhythmic locomotory cycle of any single part of the body during which the curvature is close to zero (i.e. muscles are relaxed). In some cases, small head bends corresponding to individual mid-body pulses were evident as well (**Figure 7C(i), Movie S5**).

We found the head frequency could be entrained to a range of imposed frequencies. Subjecting the mid-body to pulsed illumination at frequencies from approximately 1 to 2 Hz caused an increase in the power spectrum of the worm's oscillations at frequencies corresponding to half of the imposed frequency, and a decrease at other frequencies. Pulsing at frequencies below 1 Hz generally led to head oscillations near the imposed frequency (**Figure 7C(ii)**). These results show that a mid-body rhythmic signal can entrain head bending, and support the existence of an anteriorward coupling mechanism within the motor circuit.

We asked whether the anteriorward coupling occurs via the cholinergic neurons, which are electrically coupled to each other, the muscle-to-muscle gap junctions, or via another mechanism. We performed a similar rhythmic optogenetic inhibition pattern on the midbody cholinergic neurons. Once again, worms subject to this procedure quickly adjust their head bending frequency to match one-half of the imposed frequency (**Figure 7D(i), Movie S5**). Moreover, rhythmic illumination of the tail cholinergic neurons at 2 Hz similarly increased the magnitude of head bending at 1 Hz (**Figure 7D(ii)**). Rhythmic hyperpolarization of the mid-body

B motor neurons similarly increased the magnitude of head bending at one-half of the stimulus frequency (**Figure S7A**), as did rhythmic hyperpolarization of the BWMs when muscle-to-muscle gap junctions were disrupted by a mutation in the innexin *unc-9* (**Figure S7B**). These observations suggest that the posterior to anterior coupling is mediated neuronally, possibly by the VNC motor neurons, and not by muscle-to-muscle coupling.

DISCUSSION

In vertebrates, rhythmogenic capability for locomotion is distributed along the rostro-caudal axis of the spinal cord. In general, rostral rhythm generators are the most excitable, and recruit other rhythm generating networks into a single functional unit during locomotion. The additional, caudal oscillating units are only detectable when disconnected from their rostral partners (Kiehn, 2006).

Our results in *C. elegans* show a strikingly similar picture of forward locomotor control. We have shown that rhythmogenic capability in the worm is distributed along VNC motor circuit. As in vertebrates, however, the rhythm-generating capability of posterior circuits is only detectable when posteriorward coupling is disrupted in some manner. We showed that this disruption can take several forms: optogenetic inhibition of neurons, optogenetic inhibition of muscles (**Figure 3**), inhomogeneous mechanical environments, or lesions to the nerve cords (**Figure 5**). The incomplete nature of our optogenetic decoupling method yielded some evidence that an anterior rhythm can entrain the higher-frequency posterior rhythms, as has been described in vertebrates (Kiehn, 2006). For example, it occasionally appeared that a wave from the head, upon passing through the paralyzed region, would continue as if uninterrupted in the tail (**Figure 3B, C**).

The more striking feature of 2FU, however, was that neither the head nor tail frequency matched the natural frequency of locomotion. Instead, the normal swimming frequency in the environment of the assay was generally between these two frequencies (**Figure 7A**). This finding hints at another key similarity with models of hindlimb rhythmogenesis in mammals: during locomotion, multiple rhythm generating units are combined to form one functional unit (Kiehn, 2006). Such a whole-body oscillating unit will generally have different rhythmic properties from any subunit in isolation. Indeed, entrainment due to coupling between

oscillators normally results in a combined frequency intermediate between the two uncoupled oscillators (Giver et al., 2011). This may explain the discrepancy between the two frequencies observed during 2FU and the natural frequency of locomotion.

Our additional finding of anteriorward coupling and entrainment within the circuit is consistent with this explanation. During normal forward locomotion, the motor circuit is coupled by posteriorward proprioception (Wen et al., 2012), and additional anteriorward and posteriorward coupling mechanisms (**Figure 7**). This extensive, bidirectional coupling allows the entire circuit to operate as one unit, in much the same way that individual oscillator units in the human spinal cord are recruited to form one functional unit (Kiehn, 2006).

Our results suggest a new model of *C. elegans* forward locomotion (**Figure 8)**. Three oscillator units are depicted: an unknown head CPG, the VNC motor neurons between VB3 and AS7, and the VNC motor neurons between VB9 and the AS11. The two VNC units are justified by our data from worms in which the VNC and DNC were cut in multiple locations (**Figure 5C**). We include AS in the model because it is the only class of VNC motor neurons that we have not investigated in our 2FU assay, and could be critical to rhythm generation in the tail. These are not the only circuit units capable of generating oscillations; when we severed the VNC and DNC at arbitrary locations we found that oscillations resume closely posterior to each cut over a wide range of circuit sizes (**Figure 6**). Moreover, we could not rule out the possibility that even smaller circuit units, perhaps individual motor neurons, can give rise to rhythmic signals that are difficult to observe behaviorally.

We found to our surprise that cutting the VNC and DNC in the neck caused a severe disruption to head undulation (**Figure 5A**). Although we showed that rhythmic head bending sometimes occurred after VNC/DNC lesion, the movement we observed was of a far lower frequency than we observed in either normal locomotion or even 2FU (**Figure 5D**). One possible explanation for

this discrepancy is that input from the VNC motor neurons is essential for normal head movement. This would be consistent with the notion that all motor circuit elements are recruited into a single circuit during locomotion. However, the head motor neuron classes SMB and SMD send processes through parallel tracts that were also usually cut by our method (**Figure 5A**). Thus, we cannot rule out the possibility that damage to these neurons contributed to the disruption in head undulation.

Our discovery of a highly conserved architecture for rhythm generation in *C. elegans* sets the stage for the mechanisms for oscillator coupling and recruitment to be studied in cellular and molecular detail in this compact and manipulable model organism.

Figure 1. Overview of curvature analysis and models of rhythm generation

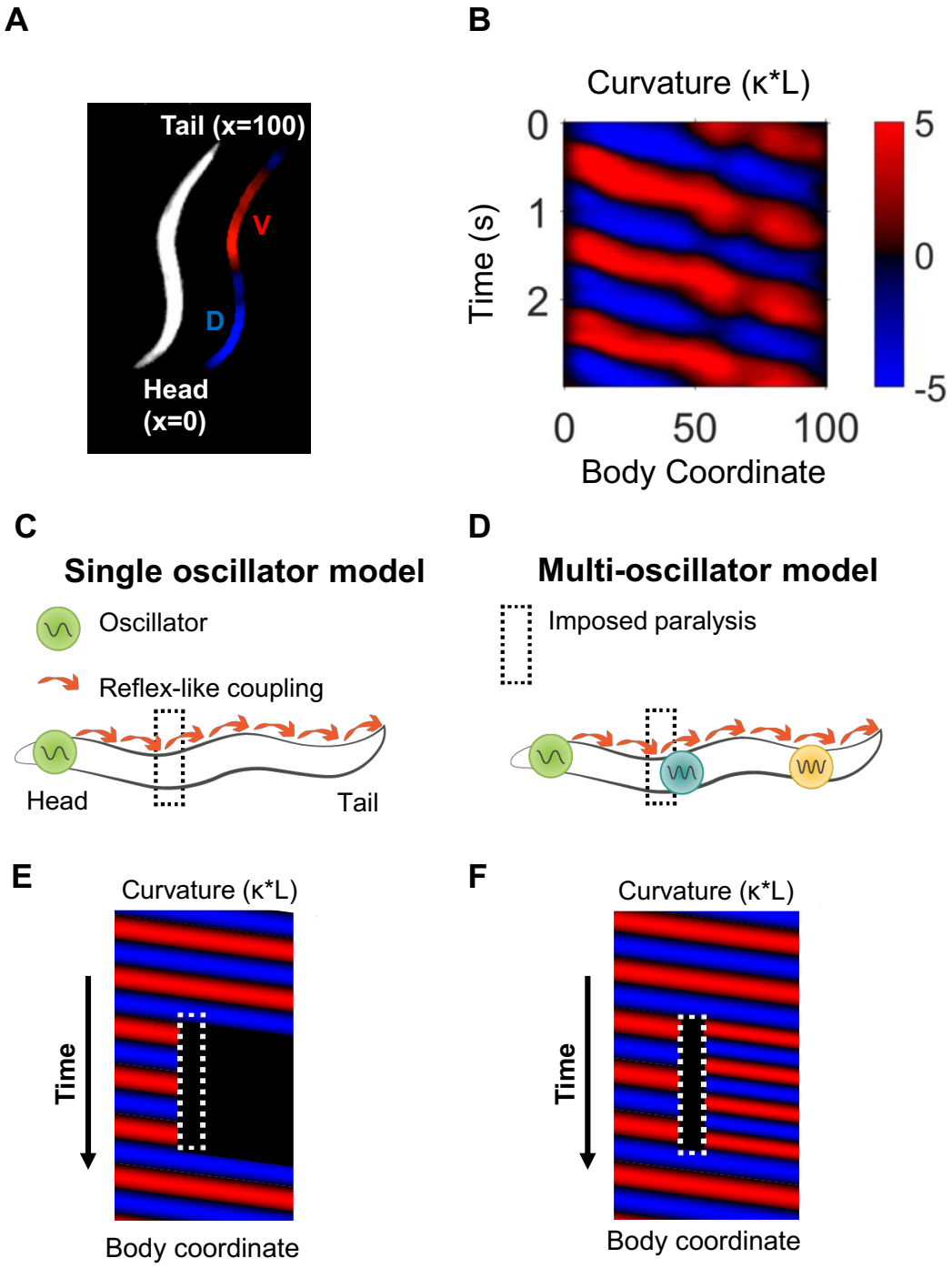

Figure 1. Overview of curvature analysis and models of rhythm generation

(A) Worm shown with curvature segmentation. Dorsal bending is shown in blue and ventral bending in red. The dorsoventral orientation is arbitrary unless otherwise specified. The worm's centerline is used to define a coordinate system in which the head and tail are located at body coordinates 0 and 100, respectively.

(B) Curvature map from the normally swimming worm in (A). The curvature at time t = 0 s corresponds to the worm orientation in (A).

(C) In a single-oscillator model of locomotion, an unknown oscillator causes rhythmic head bending, and a reflex-like coupling mechanism transduces these bends along the rest of the body.

(D) A multi-oscillator model (Gjorgjieva et al., 2014) posits the existence of additional circuit units outside the head capable of generating oscillations.

(E) Conceptual curvature map showing predicted worm behavior after paralyzing a small region of the body (dotted white box). The single-oscillator model predicts that all regions posterior to the paralyzed region will also become paralyzed.

(F) Conceptual curvature map predicting the outcome of the same manipulation applied to a multi-oscillator model. If additional oscillators exist posterior the paralyzed region, additional tail oscillations may arise, potentially with a different phase and/or frequency. See also Figure S1.

Figure 2: Anterior undulation is not required for posterior undulation

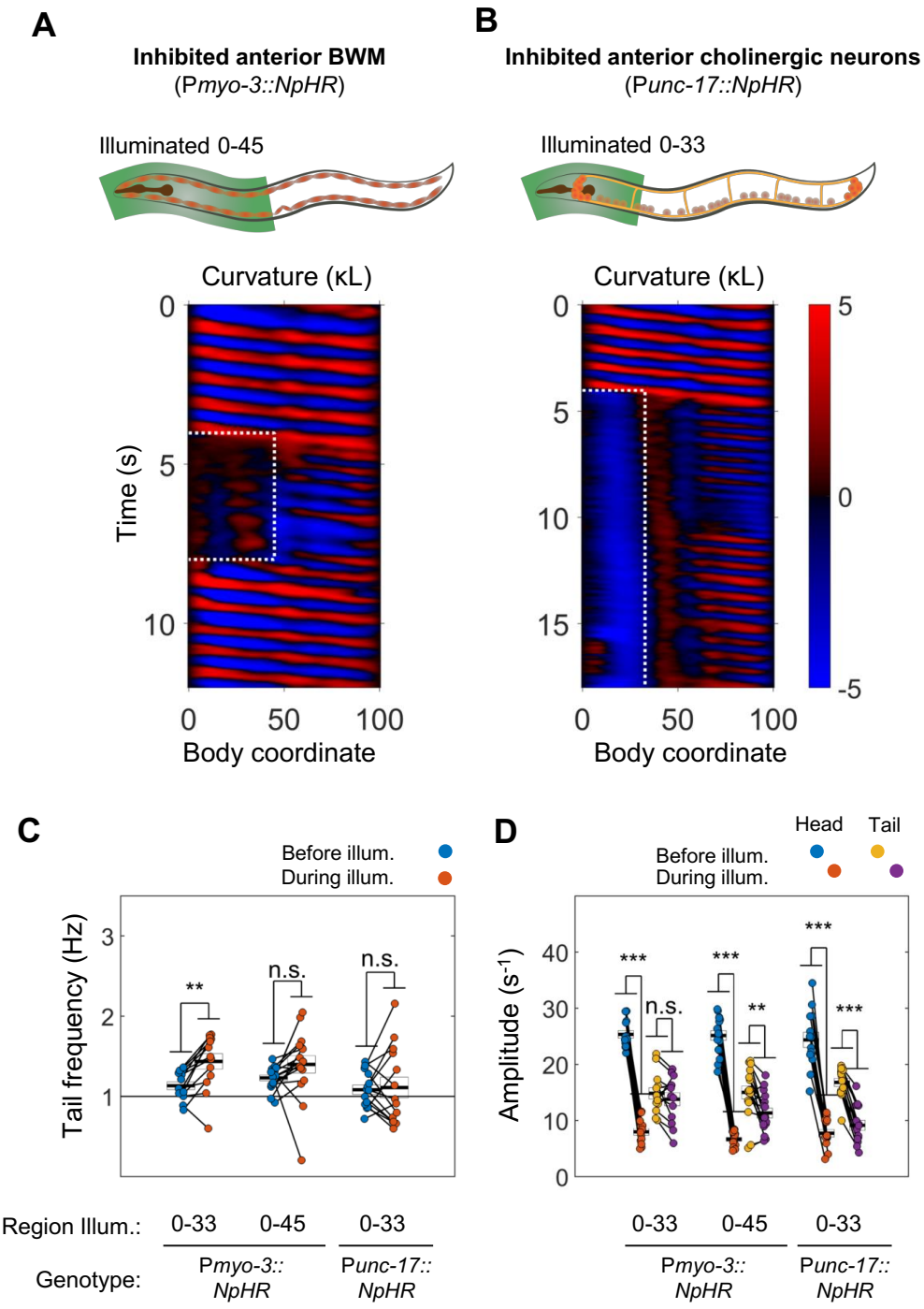

Figure 2. Anterior undulation is not required for posterior undulation

(A) Inhibition of anterior BWMs (via P*myo-3::NpHR*) increases tail frequency. Body coordinates 0-45 were illuminated with green light to trigger relaxation of the anterior muscles. The spatiotemporal extent of green laser illumination is indicated by the white dotted box.

(B) Inhibition of anterior cholinergic neurons (via P*unc-17::NpHR*; P*unc-17::ChR2*) also fails to prevent tail undulation. Body coordinates 0-33 were illuminated with green light to activate NpHR and inhibit anterior motor activity.

(C) Inhibition of some anterior muscles (0-33, N=10 worms) significantly increases tail frequency. Inhibition of most anterior muscles (0-45, N=10 worms), or inhibition of anterior cholinergic neurons (N= 14 worms) produces mixed results; some animals generate high frequency tail oscillations while others slow down. Each colored circle represents one trial; worms may have multiple trials (see methods). Tail frequency here and henceforth is measured at body coordinate 85.

(D) Amplitude of undulation in the head and tail before and during muscle or neuron inhibition. Head frequency here and henceforth is measured at body coordinate 15. Note sharp decreases in head amplitude during all three manipulations. (**) $p<0.01$; (***) $p<0.001$; paired t-test.

Figure 3: Disruption of motor coupling in the neck de-synchronizes oscillations in the head ar

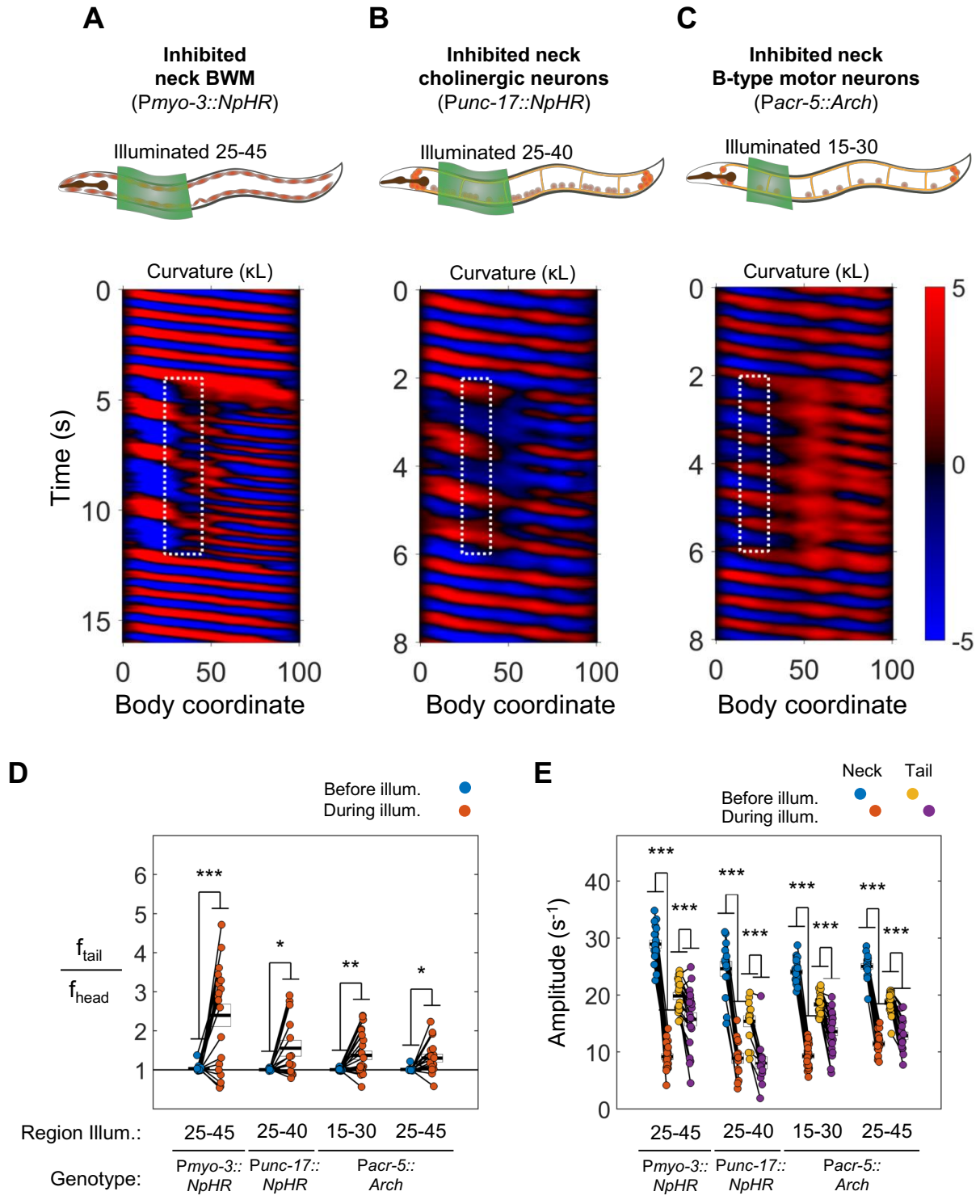

Figure 3. Disruption of motor coupling in the neck de-synchronizes head and tail oscillations

(A) Inhibition of neck BWMs (via P*myo-3::NpHR*) increases tail frequency and decreases head frequency. We refer to this decoupling as 2FU (see text). Body coordinates 25-45 were illuminated with green light to trigger relaxation of neck muscles. The spatiotemporal extent of green laser illumination is indicated by the white dotted box.

(B,C) Inhibition of neck cholinergic neurons (P*unc-17::NpHR*) or neck B-type motor neurons (Pacr-5::Arch) recapitulates the 2FU behavior seen in (A).

(D) Several optogenetic manipulations produced decoupled head and tail oscillation. 2FU is assayed by normalizing tail frequency to head frequency in each worm. Before illumination, this ratio is usually 1, indicating that the head and tail oscillate at the same frequency. During illumination, tail frequency often increases, leading to a ratio greater than 1. Each colored circle pair represents one trial; worms may have multiple trials (see methods). N= 11, 10, 12, and 10 worms per condition, respectively.

(E) Amplitude of undulation in the head and tail before and during neck muscle or neuron inhibition. Neck frequency here and henceforth is measured at body coordinate 35. (*) $p<0.05$; (**) $p<0.01$; (***) $p<0.001$; paired t-test. See also Figure S2.

Figure 4. VNC premotor interneurons, D-type motor neurons, and individual B-type motor neurons are not required for 2FU

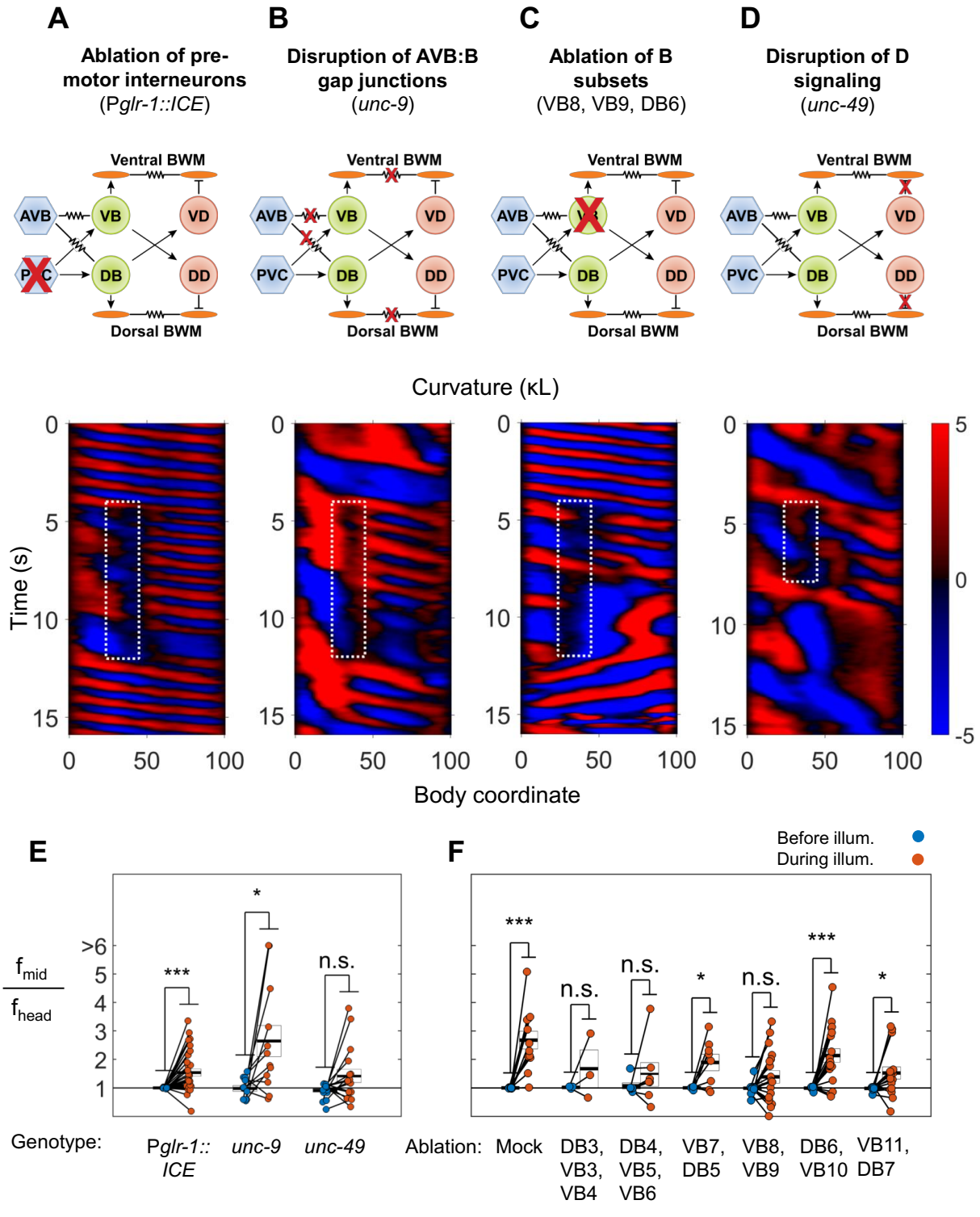

Figure 4. VNC premotor interneurons, D-type motor neuron signaling, and individual B-type motor neurons are not required for 2FU

(A) 2FU occurs despite ablation of premotor interneurons (P*glr-1::ICE*; P*myo-3::NpHR*). The spatiotemporal extent of green laser illumination is indicated by the white dotted box.

(B) 2FU occurs despite disruption of AVB:B gap junctions and BWM:BWM gap junctions (*unc-9*; P*myo-3::NpHR*)

(C) 2FU occurs despite ablation of a small subset of the B-type motor neurons (P*myo-3::NpHR*; P*acr-2::RFP)*. VB8, VB9, and DB6 were ablated using our pulsed infrared laser system (see also Figure S4E).

(D) 2FU occurs despite elimination of GABAergic signaling (*unc-49;* P*myo-3::NpHR*)

(E) When subjected to neck paralysis (P*myo-3::NpHR*; P*acr-2::RFP*), 2FU occurs reliably in P*glr-1::ICE* and *unc-9* animals and occasionally in *unc-49* animals. Each colored circle pair represents one trial; worms may have multiple trials (see methods). N= 12, 8, and 10 worms per condition, respectively. Mid-body are measured at body coordinate 55.

(F) When subjected to neck paralysis (P*myo-3::NpHR*), 2FU occurs reliably or occasionally despite ablation of subsets of the B-type motor neurons by our pulsed infrared laser system. For each condition, data is only considered from worms that have all specified neurons missing; some worms in each group may have additional B-type or other neurons missing. N= 4, 2, 2, 4, 7, 7, and 7 worms per condition, respectively. (*) $p<0.05$; (**) $p<0.01$; (***) $p<0.001$; paired t-test. See also Figures S3, S4, and S5.

Figure 5: Undulations generated in the tail after severing the dorsal and ventral nerve cords

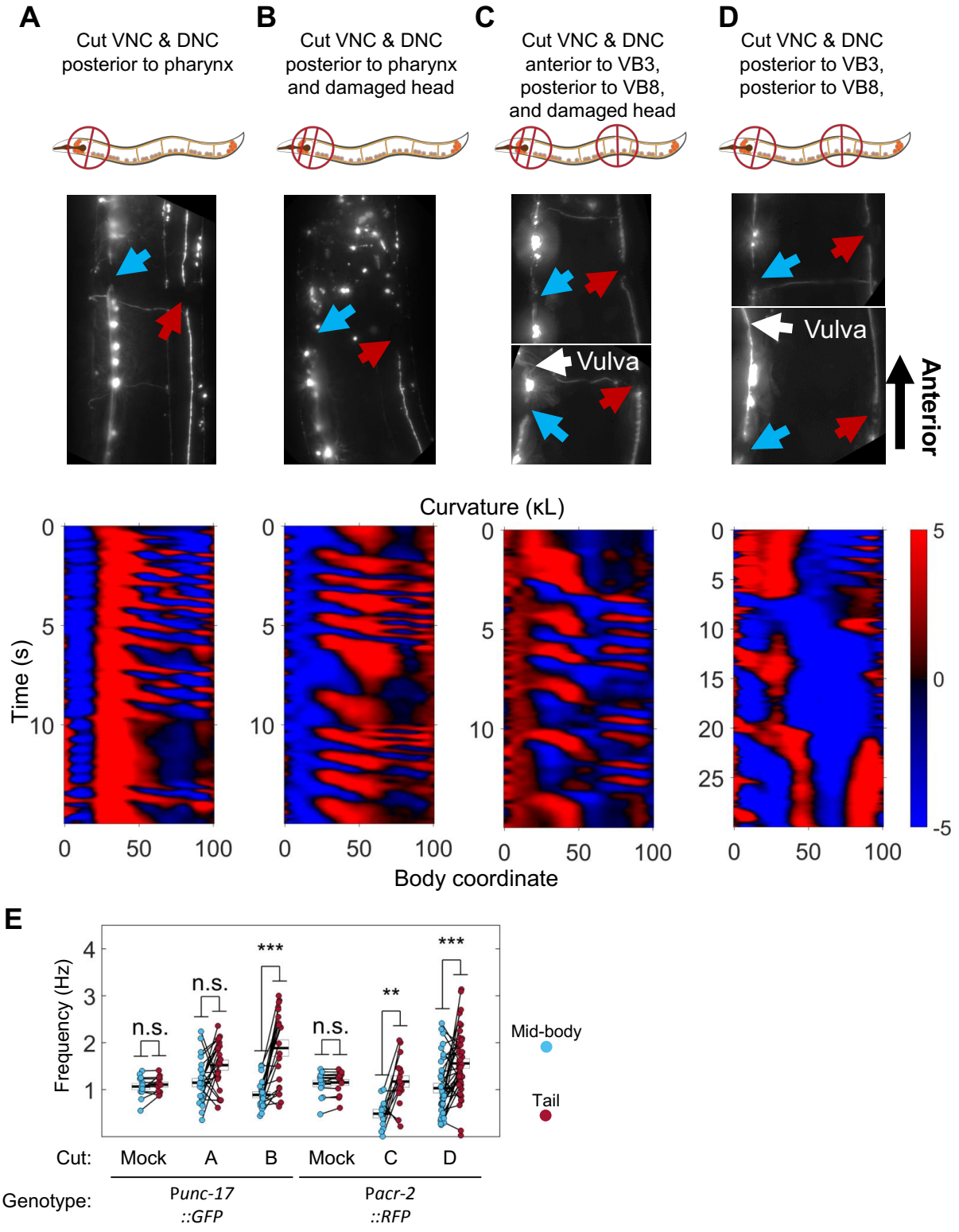

Figure 5. Undulations generated in the tail after severing the dorsal and ventral nerve cords

(A) The VNC (blue arrow) and DNC (red arrow) were severed in a P*unc-17::GFP* worm using our pulsed infrared laser system. Several other dorso-ventral processes also appear cut. Nonetheless, robust bending waves are generated in the mid-body (lower pane).

(B) The VNC and DNC are severed, and arbitrary damage has been applied to the nerve ring to suppress head movements. Robust bending waves are generated in both the neck and tail (lower pane).

(C) The VNC and DNC are severed posterior to the head and vulva (P*acr-2::RFP*), and arbitrary damage has been applied to the nerve ring to suppress head movements. Robust bending waves are generated in both the neck and tail (lower pane).

(D) The VNC and DNC are severed posterior to the head and vulva, but the nerve ring was not targeted. Low frequency head undulation and high frequency tail undulation were observed separately in this animal.

(E) Frequency of undulation in the mid-body and tail for all ablation conditions and mock controls. Each colored circle pair represents one bout of forward locomotion lasting at least 2 s. For each condition, data is only considered for worms in which the VNC and DNC are clearly severed in the indicated locations. Mid-body frequencies were measured at body coordinate 45. N = 3, 7, 3, 4, 5, and 7 worms per condition, respectively. (*) $p<0.05$; (**) $p<0.01$; (***) $p<0.001$; paired t-test. See also Figure S6.

Figure 6: Tail undulations after severing the VNC and DNC in arbitrary locations.

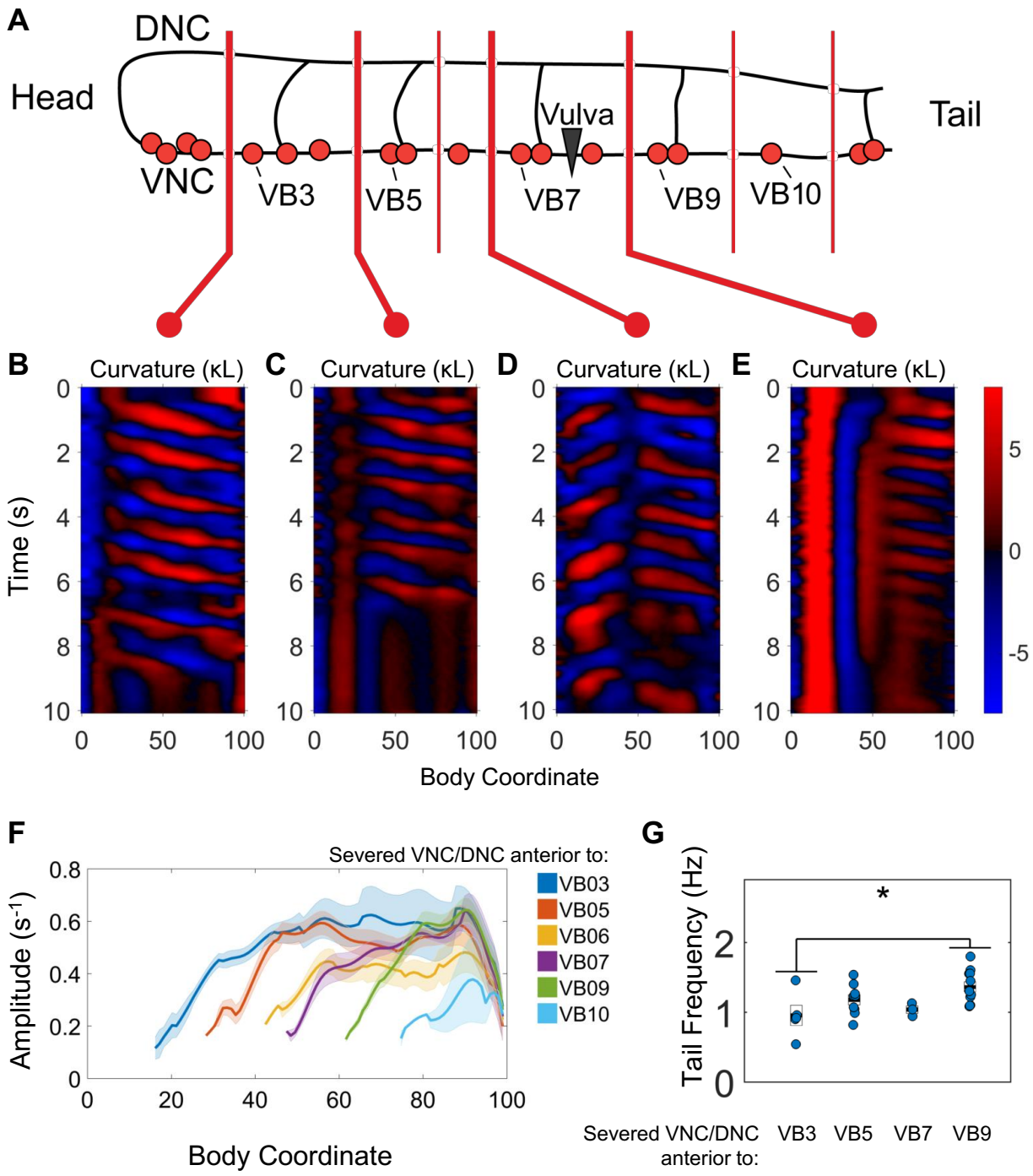

Figure 6: Undulations are generated after VNC/DNC lesioning in arbitrary locations

(A) Schematic indicating all regions at which we severed the VNC and DNC in relation to the B motor neurons. Each animal's nerve cords were severed at only one of these locations. The nerve ring of each worm was also damaged to restrict head movements as in Figure 5B.
(B-E) Representative curvature maps for worms subject to four of the tested conditions. Note that anterior-to-posterior waves begin progressively more posterior for each cut location. In some cases, the head and tail exhibited waves propagating in opposite directions (D).

(F) Amplitude of bending as a function of body coordinate after severing the VNC and DNC anterior to the indicated motor neuron. Only the portion of the curve posterior to the amplitude minima (the cut location) is shown. No bouts of locomotion with anterior-to-posterior waves were discernible posterior to the cut at VB11 either subjectively or by our analysis software. For cut locations at VB3, 5, 6, 7, 9,10, and 11 we studied N= 5, 6, 6, 11, 9, 4, and 6 worms in which we observed 8,10, 7, 5, 22, 19, and 14 bouts of forward locomotion (lasting at least 3 s), respectively. Shaded outline represents ±SEM.

(G) Frequency of undulation at body coordinate 70 for four cut conditions. Boxes represent mean and SEM. Each colored circle indicates the frequency during one bout of forward locomotion. *$p<0.05$, one-way ANOVA with Bonferroni post-hoc comparisons.

Figure 7: Head undulation frequency can be entrained by mid-body patterns

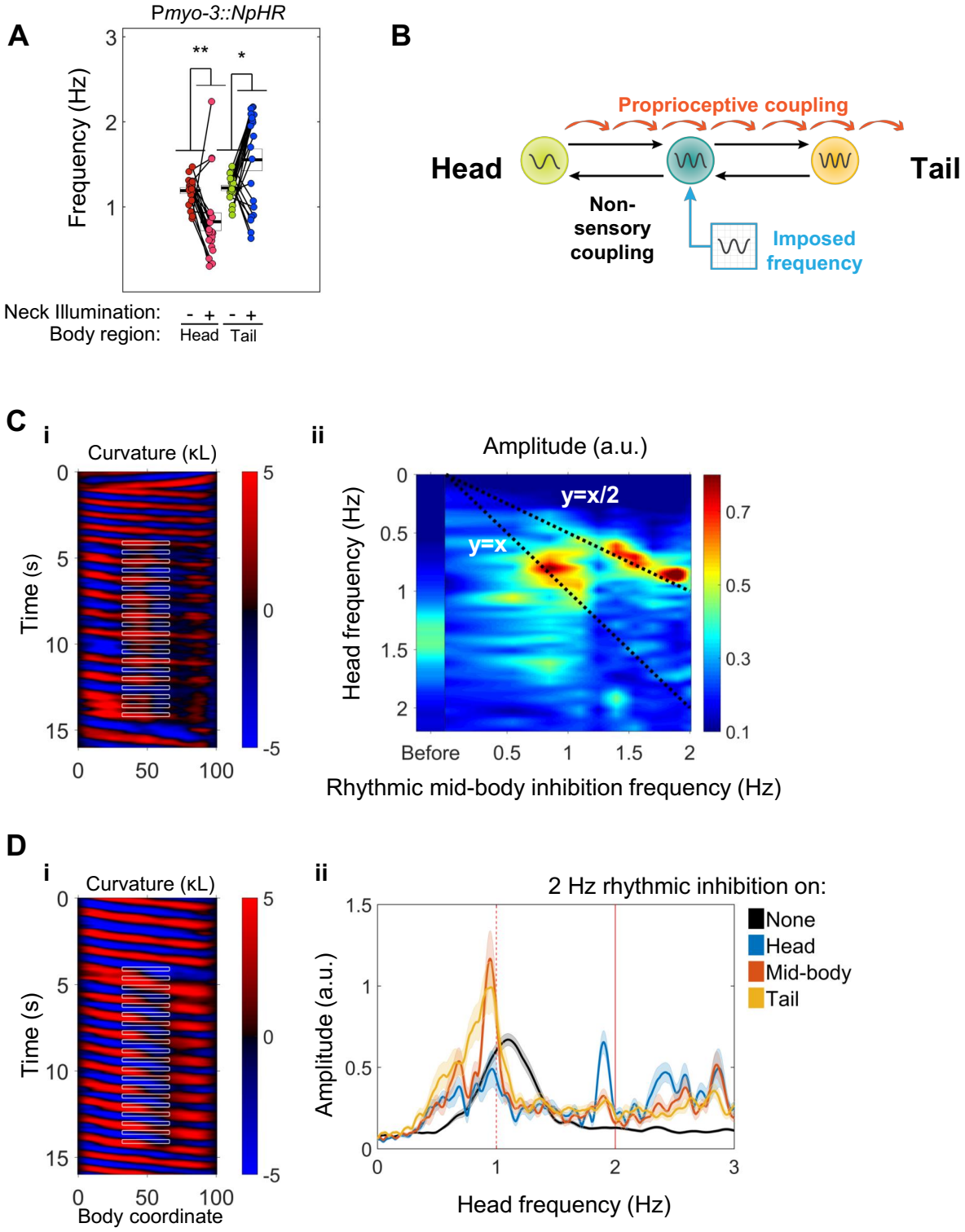

Figure 7. Head undulation frequency can be entrained by mid-body optogenetic manipulation

(A) Neck muscle hyperpolarization (Figure 3A) also causes a dramatic decrease in head bending frequency. This decrease is not predicted by either model discussed in Figure 1.

(B) A multi-oscillator model of forward locomotion allowing for motor coupling in both the anterior and posterior directions. To test this model, we sought to impose a new frequency on the mid-body of a freely moving worm, and test whether head bending also adopts the new frequency.

(C) Head bending frequency can be entrained by rhythmically inhibiting the mid-body BWMs.

(i) A curvature map showing a representative trial. Green light was pulsed on coordinates 33-66 at a frequency of 2 Hz onto a P*myo-3::NpHR* worm. Note that the head frequency slows to half of the imposed frequency, although some instances of a 1:1 correlation between laser pulse and a head bend are also evident (e.g. around t=13s).

(ii) Mean head frequency power spectra of P*myo-3::NpHR* worms before manipulation (left bar, worms from all conditions are pooled) and while subject rhythmic mid-body paralysis. Frequencies tested were 0 (with laser on), 0.5, 0.85, 1.1, 1.25, 1.4, 1.55, 1.7, 1.9, and 2.0 Hz. Frequency data is interpolated between these points. N≥11 trials per condition, with each worm supplying at most two trials. For high frequency inhibition (f>1.1 Hz) the head is entrained to half of the inhibition frequency (bright peaks lie along y=x/2). For lower frequencies of inhibition (f~0.85 Hz) the head is entrained to the inhibition frequency (bright peaks lie along y=x).

(D) Head bending frequency can be entrained by rhythmically inhibiting the head, mid-body, or tail cholinergic neurons.

(i) A curvature map showing a representative trial. Green light was pulsed on coordinates 33-66 at a frequency of 2 Hz onto a P*unc-17::NpHR* worm.

(ii) Mean head frequency spectra before manipulation (black, all conditions pooled), and after rhythmically inhibiting the head (blue, body coordinates 0-33), mid-body (orange, 33-66), or tail (yellow, 66-99) neurons at 2 Hz. Rhythmic inhibition of the mid-body or tail increases the frequency power at 1 Hz and decreases the power at the original undulation frequency, mirroring (C). N≥16 trials per condition, with each worm supplying at most two trials. Shaded outlines are the SEM. Vertical red lines indicate the imposed frequency (solid) or one-half of the imposed frequency (dashed). See also Figure S7.

Figure 8: Overview of forward locomotion

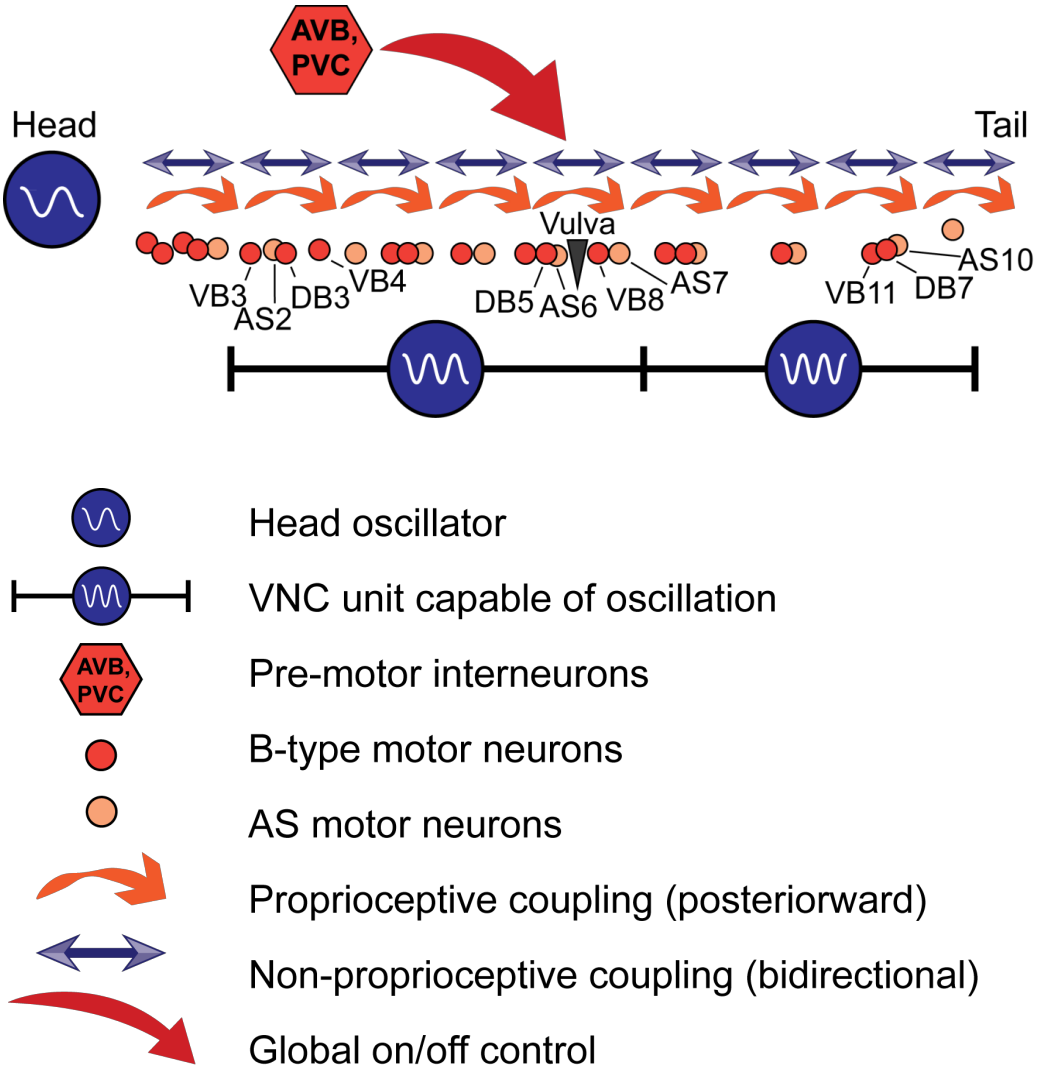

Figure 8. A model for *C. elegans* forward locomotion

Two units of the VNC motor neurons (and potentially more subsections) are capable of independent rhythm generation. However, all oscillating units are coupled by proprioceptive coupling (Wen et al., 2012) and another unknown, likely non-proprioceptive coupling mechanism that allows communication in the anteriorward direction, and potentially in the posteriorward direction. Pre-motor interneurons may activate or suppress this circuit, but are not required for rhythm generation or propagation.

MATERIALS AND METHODS

Strains

We maintained *C. elegans* on 6 cm NGM plates seeded with *E. coli* OP50 at 20˚C using standard methods (Sulston and Hodgkin, 1988). For all optogenetic experiments, we added 100mM all-trans retinal (ATR) in ethanol at 0.8% by volume to the bacteria suspension before seeding the plates, and kept plates in darkness. All strains were synchronized by bleaching and allowed to hatch on an NGM plate without food. L1 arrested larvae were transferred to OP50 or OP50+ATR plates and allowed to grow to the appropriate stage. Unless otherwise specified, all experiments were performed using adult hermaphrodites.

All strains used in this study are listed in Tables S1 and S2. Transgenic strains were outcrossed a minimum of 3 times against N2.

Construction and validation of the optogenetic targeting system

We constructed an optogenetic targeting system similar to that described in Leifer et al (2011) based around a Leica DMI4000B microscope. Dark field illumination is provided by red LEDs and worms were imaged by an sCMOS camera (QImaging optiMOS). Custom written C++ software performs image segmentation of the worm and allows the user to select a region of the worm to illuminate. The illumination region is sent to a digital micromirror device (DMD), which then projects the laser onto only the desired portion of the worm through a 10X objective. The entire cycle runs at 40 Hz. A green laser with 532 nm wavelength (GL532T3-300, irradiance 10 mW/mm^2 at focal plane, Shanghai Laser & Optics Century) was used for all activations of NpHR or Arch, and a blue 473 nm wavelength laser (BL473T3-150, irradiance 4 mW/mm^2 at focal plane, Shanghai Laser & Optics Century) was used for activation of ChR2. Worms were placed

in a 17% dextran solution (Fang-Yen et al., 2010) in an 80 μm thick chamber between a slide and a coverglass placed on the microscope stage.

To determine the accuracy of our setup, we studied worms that express the excitatory opsin ChR2 under the control of the *aptf-1* promoter. These worms were reported to quickly become quiescent when the RIS head neuron is illuminated with blue light (Turek et al., 2013). We targeted a thin band of blue light to various locations along the centerline of each worm, and measured the amplitude of head bending waves as an output (data not shown). The distance between the region where most slowing occurred (Body coordinate 14) and the nearest region with no slowing (Body coordinate 20) suggests that our variant has a resolution of at least 6% of an adult worm's body length. The original targeting system's resolution was measured by an optogenetic egg-laying assay, and was also estimated at about 6% of a worm's body length (Leifer et al., 2011).

Optogenetic inhibition and stimulation

For head and neck optogenetic inhibition experiments, YX9 (Muscle::NpHR), ZM5016 (Cholinergic Neurons::NpHR), WEN001 (B::Arch) , YX127 (Cholinergic Neurons:: NpHR&ChR2, A/VC::miniSOG), YX119 (Muscle::NpHR, *unc-49*(*e407*)), YX137 (Muscle::NpHR, *unc-7*(*e5*)), or YX140 (Muscle::NpHR, *unc-9*(*fc16*)) larvae were transferred to ATR plates and allow to grow for 3 days, reaching the first day of adulthood. Up to 20 adult worms were mounted at a time on our optogenetic targeting system. Worms were sampled with replacement from the dextran chamber, and illuminated with a 532 nm laser a total of 1-3 times in the indicated region, with at least 10 s between successive illuminations of the same animal.

For activation of posterior B and AS motor neurons, YX127 (Cholinergic neurons::NpHR&ChR2, A/VC::miniSOG) worms were allowed to grow to the second larval stage on ATR plates, and then illuminated *en masse* with blue light (470±17nm) at 3 mW/mm^2 for 20 minutes to ablate the

A-type motor neurons. Worms were transferred to a fresh OP50+ATR plate to grow for 2 more days. To ensure a loss of reversal capability in each day 1 adult, worms were individually prodded with a platinum wire. All worms tested failed to move backwards during this assay. Worms were then mounted on the optogenetic targeting system as before. Global amber (580±15nm) illumination was applied through the transmitted light port of the microscope and varied in irradiance until just strong enough to paralyze the worm, presumably through the action of P*unc-17::NpHR*. Once paralyzed or nearly paralyzed, 473 nm laser light was applied to the indicated region of the tail using the DMD.

For rhythmic inhibition of muscles or cholinergic neurons, synchronized YX148 (Muscle::NpHR, AB::RFP) L4 larvae, YX139 (Muscle::NpHR, BWM gap junctions disrupted) L4 larvae, YX127 day 1 adults, or WEN001, day 1 adults grown on ATR plates were mounted on the optogenetic targeting system and illuminated periodically at the indicated frequency and location through our custom software. For this experiment, L4 *qhIs1* larvae were used because expression of *myo-3::NpHR::ECFP* in the BWMs appeared to be weaker in adults. YX127 animals were not exposed to blue light prior to this experiment.

Neuron photoablation using miniSOG

For optogenetic 2FU experiments, YX126 (Muscle::NpHR, A/VC::miniSOG) larvae were allowed to grow for 2 days on OP50 plates until the L4 stage, at which RFP was visible in the both the A- and VC-type motor neurons. Worms were bulk illuminated with blue light (wavelength 470±17 nm) at 3.5 mW/mm^2 for 20 minutes of total illumination time using 0.5 s on / 1.5 s off pulse train from a Leica EL6000 light source. After illumination, the larvae were transferred to OP50+ATR plates, and incubated for 2 additional days, but did not appear to grow past the L4 stage. Control worms were handled identically except for the blue illumination, and were not analyzed. During the optogenetic experiments, each worm was recorded attempting at least one reversal;

none successfully moved backwards. In addition, worms were handled individually and recovered from the dextran chamber for fluorescence imaging. We mounted each worm on a separate 4% agar pad and acquired RFP images on a compound fluorescence microscope (Leica DMI6000B). In control worms, which grew into adults, RFP was visible in the VC-type motor neurons, some A-type motor neurons (RFP was visible in all A-type motor neurons at the L2-L4 stages), and the posterior intestine. The normal RFP expression pattern in A- and VC-type motor neuron was absent in all illuminated worms. However, neurons in the tail corresponding to VA12, DA8, or DA9 were usually visible (see also Figure S6A).

For VNC/DNC cauterization experiments, YX177 (AB::RFP, A/VC::miniSOG) worms were exposed to blue light at the L2 stage using 0.5 s on / 1.5 s off pulsing and surgically manipulated at the day 2 adult stage as described below. Ablation of the A motor neurons was assessed by recording GFP fluorescence images of each animal after behavioral imaging. In all animals, only B and AS motor neurons were visible along most of the VNC, with the exception of the same three posterior A motor neurons noted above.

Ablation of premotor interneurons by ICE

Prior to conducting optogenetic experiments, we generated strains YX152 (P*nmr-1::ICE*; P*glr-1::ChR2::YFP*) and YX153 (P*glr-1::ICE*; P*glr-1::ChR2::YFP*) to test whether the interneurons were appropriately ablated. Control ZM4624 (P*glr-1*::ChR2::YFP) L1 larvae and adults showed bright YFP labeling of many neurons, including many head neurons and PVC, which was the only pair of labeled neurons in the tail.

In L1 arrested YX152 and YX153 worms, many neurons were also easily visualized by YFP, although normal locomotion was impaired. By the adult stage, YFP signals in all head and tail neurons had nearly vanished in all YX153 worms (N=18); some small and faint fluorescent puncta, similar in appearance to intestinal birefringent granules, were visible in the nerve ring

and tail. These dim puncta did not have visible processes, and we were unable to identify any head neurons or PVC in any of these worms. In YX152 adults, PVC was similarly not identifiable in any worm (N=10), although many brightly YFP-labeled neurons were visible in the nerve ring. These results suggest that all or most P*glr-1* positive interneurons are ablated in P*glr-1*::ICE worms and that PVC (and likely other P*nmr-1* positive neurons) are ablated in P*nmr-1::ICE* worms. AVB may still be present in both YX152 and YX153 (Kawano et al., 2011; Kawano, Po, and Zhen, unpublished).

For optogenetic experiments, we generated strains YX159 (Muscle::NpHR, IN::ICE) and YX160 (Muscle::NpHR, IN::ICE) and performed optogenetic illuminations as in our original optogenetic 2FU experiments.

Pulsed infrared laser cauterization of motor neurons and nerve cords

For ablation of B motor neurons, YX148 (Muscle::NpHR, AB::RFP) worms were raised on ATR plates until most animals were at the L3 to L4 stage, and then immobilized on 4% agar pads by 50 nm polystyrene beads (Kim et al., 2013). Each pad was mounted on a pulsed infrared laser system (Churgin et al., 2013) that had been modified with increased power to deliberately kill cells. Each neuron, visualized by P*acr-2::RFP*, was irradiated with a single 0.8 to 1.6 ms pulse of the 400 mW laser through a 63X oil immersion objective. We determined that a single 0.8 ms pulse reliably kills the targeted VNC motor neuron, has a 50% chance of killing a VNC neighbor within 2.5 µm, and has a 10% chance of killing a VNC neighbor within 5 µm from the target (A. D. F. and C. F.-Y., unpublished data). After ablation, worms were recovered and transferred to a fresh ATR plate to resume development for 1 additional day. During optogenetic experiments, worms were handled individually and recovered to agar pads after illumination. We then acquired RFP fluorescence images of each animal through a 40X objective on a compound

fluorescence microscope (Leica DMI 6000B). Images were examined manually, and A- and B-type motor neurons were labeled as present or missing based on the stereotypic ordering, commissural orientation, and the presence or absence of commissures from dorsal A- or B-type motor neurons. In each category in Figure 5F, we included only worms for which all indicated B motor neurons were missing. Some individuals in each category had additional missing neurons. In Figures S4 and S5, all ablated B motor neurons are indicated for each individual worm example.

To sever the VNC and DNC, day 2 adult YX148 or LX929 (Cholinergic neuron::GFP) worms were immobilized with polystyrene beads and mounted on our infrared laser system as before, and the indicated area of the RFP- or GFP-labeled cord was illuminated with a train of 10-25 2ms pulses. Worms were transferred to fresh OP50 plates and allowed to recover for at least four hours before behavioral and fluorescence imaging. For behavioral imaging, worms were mounted individually in 20% dextran chambers and recorded swimming for at least 1 minute under dark field illumination. Because these worms were generally not active (especially when the VNC and DNC were lesioned in two locations), we mechanically vibrated them at about 200 Hz using a cell phone motor for periods of 10-20 s to induce locomotion at least twice during each recording. After behavioral imaging, each worm was transferred to a pad and imaged for red or green fluorescence through a 63X objective at the appropriate regions (neck or mid-body). Images were examined manually, and data was only analyzed from worms in which all indicated nerve cord locations appeared completely severed.

Head lesions using a heated wire

To broadly lesion the head and inhibit anterior bending, four freely crawling adult N2 worms were gently touched on or near the head with a platinum wire attached to a soldering iron. The

worms appeared to crawl backwards after the initial touch, so we applied a second touch to the agar near the tail to induce forward locomotion. We recorded behavior immediately after lesioning.

Heterogenous mechanical environment experiments

Day 1 adult N2 worms were transferred in low viscosity NGM buffer (NGMB) to a slide containing 3 to 5 µL islands of solutions of high viscosity 3% HPMC (Ashland Benecel K200M) in NGMB. A second slide, spaced by 125 µm thick plastic spacers, was placed on top to form a 2-dimensional chamber similar to those used for optogenetics experiments, but with an inhomogeneous mechanical environment. We imaged each slide under dark field illumination on a Nikon TE2000-S microscope and recorded worms transitioning from the low viscosity to high viscosity regions.

Curvature segmentation, analysis, and statistics

For experiments in which worms were recorded with our optogenetic targeting system, the segmentation computed live for body targeting was recorded to disk along with each video frame. We wrote custom MATLAB codes to compute the curvature of the worm in each frame using the recorded centerline coordinates.

For all other experiments, worm segmentations were generated from dark field videos using WormLab (MBF Bioscience, Williston, VT). The centerline coordinates were exported and curvature maps were constructed as before. To identify bouts of forward locomotion in 1-2 min worm recordings, we computed the activity level and wave direction in the kymogram as a function of both time and body coordinate. Bouts of forward locomotion in body segments were

identified when the activity level was higher than fixed threshold and the local direction of wave propagation was anterior-to-posterior for longer than the amount of time specified (typically 2-3 s).

To measure frequencies of undulation at any body coordinate, we computed the Fourier transform of time differentiated curvature, and used the frequency corresponding to the peak amplitude. Bending amplitudes are the root mean square of time differentiated curvature. Changes in the mean frequency, frequency ratio, or bending amplitude of all paired data are evaluated by the paired t-test.

KEY RESOURCES TABLE

Table 1: Transgenic arrays acquired or generated for this study

Strain	Plasmid or Reference	Description	Purpose	Transgene
LX929	(Chase et al., 2004)	*Punc-17::GFP*	Identification of VNC and DNC	*vsIs48*
VM4770	(Zheng et al., 1999)	P*nmr-1::ICE; lin-15(+)*	Ablation of INs	*akIs11*
VM4771	(Zheng et al., 1999)	P*glr-1::ICE; lin-15(+)*	Ablation of INs	*kyIs36*
WEN001	pJH2918	P*acr-5::ArchT::RFP; lin-15(+)*	Inhibition of B motor neurons	*wenIs001*
YX9	(Leifer et al., 2011)	P*myo-3::NpHR::ECFP; lin-15(+)*	Inhibition of muscles	*qhIs1*
YX10				*qhIs2*
YX146	pJH1841	P*acr-2::wCherry; dpy-20(+)*	Identification of B	*qhIs4*
ZM2509	(Wen et al., 2012)	*unc-9(fc16); hpIs3;* P*rgef-1-unc-9cDN) + odr-1*	Neuronal *unc-9* rescue	*hpEx803*
ZX460/ ZM3265	(Liewald et al., 2008)	P*unc-17::ChR2(H134R)::YFP; lin-15(+)*	Stimulation of cholinergic neurons	*zxIs6*
ZM4624	(Gao et al., 2015)	P*glr-1::chop-2(H134R)::YFP; lin-15(+)*	Identification of INs	*hpIs166*
ZM5016	(Leifer et al., 2011)	P*unc-17::NpHR::ECFP; lin-15(+)*	Inhibition of cholinergic neurons	*hpIs178*
ZM7690	pJH2843	P*unc-4::tomm-20::miniSOG:: urSL::wCherry; lin-15(+)*	Ablation of A and VC	*hpIs366*
ZM7691				*hpIs371*

Table 2: Additional strains generated using the above arrays

Strain Name	Genotype	Description
YX119	*qhIs1; unc-49(e407)*	Muscle::NpHR, *unc-49*
YX126	*qhIs1; hpIs371*	Muscle::NpHR, A/VC::miniSOG
YX127	*hpIs178; hpIs371; zxIs6*	Cholinergic Neurons::NpHR&ChR2, A/VC::miniSOG
YX137	*qhIs1; unc-7(e5)*	Muscle::NpHR, *unc-7*
YX139	*qhIs1; unc-9(fc16); hpEx803*	Muscle::NpHR, UNC-9 disruption in muscles only
YX140	*qhIs1; unc-9(fc16)*	Muscle::NpHR, *unc-9*
YX148	*qhIs1; qhIs4*	Muscle::NpHR, AB::RFP
YX152	*hpIs166; akIs11*	IN::ICE&YFP
YX153	*hpIs166; kyIs36*	IN::ICE&YFP
YX159	*qhIs2; akIs11*	Muscle::NpHR, IN::ICE
YX160	*qhIs2; kyIs36*	Muscle::NpHR, IN::ICE
YX177	*hpIs366; vsIs48*	A/VC::miniSOG, Cholinergic Neurons::GFP

MOVIE TITLES

Movie S1: Posterior undulations after anterior paralysis

Movie S2: Two-frequency undulation

Movie S3: Additional manipulations that evoke two-frequency undulation

Movie S4: Posterior undulations after severing the VNC and DNC

Movie S5: Head undulation frequency can be entrained by mid-body optogenetic manipulation

AUTHOR CONTRIBUTIONS

A. D. F. and C. F.-Y. conceived and designed experiments and wrote the manuscript. All authors edited or approved the manuscript. All authors performed experiments, analyzed data, or contributed unpublished reagents.

ACKNOWLEDGEMENTS

We thank Quan Wen, Min Wu, Michelle Po, Yishi Jin, Andres Villu Mariq, and Alexander Gottschalk for providing strains. Some strains were provided by the by the CGC, which is funded by NIH Office of Research Infrastructure Programs (P40 OD010440). C. F.-Y. was supported by the National Institutes of Health, Ellison Medical Foundation, and Sloan Research Foundation. A. D. F. was supported by the National Institutes of Health. S. T. was supported by an Abraham Noordergraaf Research Fellowship. J. R. M. was supported by a Holtz Undergraduate Research Fellowship. M. Zhen was supported by the Canadian Institute of Health Research. We thank David Raizen, Vijay Balasubramanian, Robert Kalb, Gal Haspel, and Brian Chow for helpful suggestions and discussions, Matthew Churgin for technical assistance, and Wassana Techadilok for assistance with figure preparation.

REFERENCES

Ahringer, J. (2006). Reverse Genetics. In WormBook.

Altun, Z.F., and Hall, D.H. (2011). Nervous system, general description. In WormAtlas.

Bamber, B.A., Beg, A.A., Twyman, R.E., and Jorgensen, E.M. (1999). The Caenorhabditis elegans unc-49 Locus Encodes Multiple Subunits of a Heteromultimeric GABA Receptor. The Journal of Neuroscience 19, 5348-5359.

Chalfie, M., Sulston, J., White, J., Southgate, E., Thomson, J., and Brenner, S. (1985). The Neural Circuit for Touch Sensitivity in Caenorhabditis elegans. The Journal of Neuroscience 5, 956-964.

Chase, D.L., Pepper, J.S., and Koelle, M.R. (2004). Mechanism of extrasynaptic dopamine signaling in *Caenorhabditis elegans*. Nat Neurosci 7, 1096-1103.

Churgin, M.A., He, L., Murray, J.I., and Fang-Yen, C. (2013). Efficient Single-Cell Transgene Induction in Caenorhabditis elegans Using a Pulsed Infrared Laser. G3: Genes|Genomes|Genetics 3, 1827-1832.

Duerr, J.S., Han, H.P., Fields, S.D., and Rand, J.B. (2008). Identification of major classes of cholinergic neurons in the nematode Caenorhabditis elegans. The Journal of comparative neurology 506, 398-408.

Evans, T.C. (2006). Transformation and microinjection. WormBook.

Fang-Yen, C., Wyart, M., Xiea, J., Kawaia, R., Kodgere, T., Chena, S., Wen, Q., and Samuel, A.D.T. (2010). Biomechanical analysis of gait adaptation in the nematode Caenorhabditis elegans. Proceedings of the National Academy of Sciences 107, 20323–20328.

Flytzanis, N.C., Bedbrook, C.N., Chiu, H., Engqvist, M.K.M., Xiao, C., Chan, K.Y., Sternberg, P.W., Arnold, F.H., and Gradinaru, V. (2014). Archaerhodopsin Variants with Enhanced Voltage Sensitive Fluorescence in Mammalian and Caenorhabditis elegans Neurons. Nature communications 5, 4894-4894.

Gao, S., Xie, L., Kawano, T., Po, M.D., Pirri, J.K., Guan, S., Alkema, M.J., and Zhen, M. (2015). The NCA sodium leak channel is required for persistent motor circuit activity that sustains locomotion. Nat Commun 6.

Giver, M., Jabeen, Z., and Chakraborty, B. (2011). Phase and frequency entrainment in locally coupled phase oscillators with repulsive interactions. Physical Review E 83, 046206.

Gjorgjieva, J., Biron, D., and Haspel, G. (2014). Neurobiology of Caenorhabditis elegans Locomotion: Where Do We Stand? BioScience 64, 476-486.

Grillner, S. (2003). The motor infrastructure: from ion channels to neuronal networks. Nat Rev Neurosci 4, 573-586.

Haspel, G., O'Donovan, M.J., and Hart, A.C. (2010). Motorneurons dedicated to either forward or backward locomotion in the nematode C. elegans. The Journal of neuroscience : the official journal of the Society for Neuroscience 30, 11151-11156.

Husson, S.J., Liewald, J.F., Schultheis, C., Stirman, J.N., Lu, H., and Gottschalk, A. (2012). Microbial Light-Activatable Proton Pumps as Neuronal Inhibitors to Functionally Dissect Neuronal Networks in C. elegans. PLoS ONE 7, e40937.

Karbowski, J., Schindelman, G., Cronin, C., Seah, A., and Sternberg, P. (2008). Systems level circuit model of C. elegans undulatory locomotion: mathematical modeling and molecular genetics. J Comput Neurosci 24, 253-276.

Kawano, T., Po, Michelle D., Gao, S., Leung, G., Ryu, William S., and Zhen, M. (2011). An Imbalancing Act: Gap Junctions Reduce the Backward Motor Circuit Activity to Bias C. elegans for Forward Locomotion. Neuron 72, 572-586.

Kerr, R. (2006). Imaging the activity of neurons and muscles. WormBook, ed. (The C. elegans Research Community).

Kerr, R., Lev-Ram, V., Baird, G., Vincent, P., Tsien, R.Y., and Schafer, W.R. (2000). Optical Imaging of Calcium Transients in Neurons and Pharyngeal Muscle of C. elegans. Neuron 26, 583-594.

Kiehn, O. (2006). Locomotor circuits in the mammalian spinal cord. Annual Review of Neuroscience 29, 279-306.

Kim, E., Sun, L., Gabel, C.V., and Fang-Yen, C. (2013). Long-Term Imaging of Caenorhabditis elegans Using Nanoparticle-Mediated Immobilization. PLoS ONE 8, e53419.

Kocabas, A., Shen, C.-H., Guo, Z., and Ramanathan, S. (2012). Controlling interneuron activity in Caenorhabditis elegans to evoke chemotactic behaviour. Nature 490, 273-278.

Lai, C.-H., Chou, C.-Y., Ch'ang, L.-Y., Liu, C.-S., and Lin, W.-c. (2000). Identification of Novel Human Genes Evolutionarily Conserved in Caenorhabditis elegans by Comparative Proteomics. Genome Research 10, 703-713.

Leifer, A.M., Fang-Yen, C., Gershow, M., Alkema, M.J., and Samuel, A.D.T. (2011). Optogenetic manipulation of neural activity in freely moving Caenorhabditis elegans. Nat Meth 8, 147-152.

Liewald, J.F., Brauner, M., Stephens, G.J., Bouhours, M., Schultheis, C., Zhen, M., and Gottschalk, A. (2008). Optogenetic analysis of synaptic function. Nat Meth 5, 895-902.

Liu, Q., Chen, B., Gaier, E., Joshi, J., and Wang, Z.W. (2006). Low conductance gap junctions mediate specific electrical coupling in body-wall muscle cells of Caenorhabditis elegans. J Biol Chem 281.

Marder, E., Bucher, D., Schulz, D.J., and Taylor, A.L. (2005). Invertebrate Central Pattern Generation Moves along. Current Biology 15, R685-R699.

Marder, E., and Calabrese, R.L. (1996). Principles of rhythmic motor pattern generation. Physiological Reviews 76, 687-717.

McIntire, S., Jorgensen, E., and Horvitz, H. (1993a). Genes required for GABA function in Caenorhabditis elegans. Nature 364, 334-337.

McIntire, S., Jorgensen, E., Kaplan, J., and Horvitz, H. (1993b). The GABAergic nervous system of Caenorhabditis elegans. Nature 364, 337-341.

Pierce-Shimomura, J.T., Chen, B.L., Mun, J.J., Ho, R., Sarkis, R., and McIntire, S.L. (2008). Genetic analysis of crawling and swimming locomotory patterns in C. elegans. Proceedings of the National Academy of Sciences 105, 20982-20987.

Starich, T.A., Xu, J., Skerrett, I.M., Nicholson, B.J., and Shaw, J.E. (2009). Interactions between innexins UNC-7 and UNC-9 mediate electrical synapse specificity in the Caenorhabditis elegans locomotory nervous system. Neural Development 4, 16.

Stirman, J., Crane, M., Husson, S.J., Wabnig, S., Schultheis, C., Gottschalk, A., and Lu, H. (2011). Real-time multimodal optical control of neurons and muscles in freely behaving Caenorhabditis elegans. Nature Methods 8, 153-159.

Sulston, J., and Hodgkin, J. (1988). Methods. In The Nematode Caenorthabditis elegans, W.B. Wood, ed. (Cold Spring Harbor, NY: Cold Spring Harbor Laboratory Press).

Turek, M., Lewandrowski, I., and Bringmann, H. (2013). An AP2 Transcription Factor Is Required for a Sleep-Active Neuron to Induce Sleep-like Quiescence in C. elegans. Current Biology 23, 2215-2223.

Varshney, L.R., Chen, B.L., Paniagua, E., Hall, D.H., and Chklovskii, D.B. (2011). Structural Properties of the <italic>Caenorhabditis elegans</italic> Neuronal Network. PLoS Comput Biol 7, e1001066.

Waggoner, L.E., Zhou, G.T., Schafer, R.W., and Schafer, W.R. (1998). Control of Alternative Behavioral States by Serotonin in Caenorhabditis elegans. Neuron 21, 203-214.

Wen, Q., Po, M.D., Hulme, E., Chen, S., Liu, X., Wai, S., Kwok, Gershow, M., Leifer, A.M., Butler, V.*, et al.* (2012). Proprioceptive Coupling within Motor Neurons Drives C. elegans Forward Locomotion. Neuron 76.

White, J., Southgate, E., Thomson, J., and Brenner, S. (1986). The Structure of the Nervous System of the Nematode Caenorhabditis elegans. Philosophical Transactions of the Royal Society of London B 314, 1-340.

White, J.G., Southgate, E., Thomson, J.N., and Brenner, S. (1976). The Structure of the Ventral Nerve Cord of Caenorhabditis elegans. Philosophical Transactions of the Royal Society of London B, Biological Sciences 275, 327-348.

Wicks, S., and Rankin, C. (1995). Integration of mechanosensory stimuli in Caenorhabditis elegans. The Journal of Neuroscience 15, 2434-2444.

Zhang, F., Wang, L.-P., Brauner, M., Liewald, J.F., Kay, K., Watzke, N., Wood, P.G., Bamberg, E., Nagel, G., Gottschalk, A., and Deisseroth, K. (2007). Multimodal fast optical interrogation of neural circuitry. Nature 446, 633-639.

Zhen, M., and Samuel, A. (2015). C. elegans locomotion: small circuits, complex functions. Current Opinion ini Neurobiology 33, 117-126.

Zheng, Y., Brockie, P.J., Mellem, J.E., Madsen, D.M., and Maricq, A.V. (1999). Neuronal Control of Locomotion in C. elegans Is Modified by a Dominant Mutation in the GLR-1 Ionotropic Glutamate Receptor. Neuron 24, 347-361.

Supplemental Information

Figure S1. Related to Figure 2. Tail undulation after gross head lesioning

The approximate location of hot wire lesioning is indicated with a red arrow. Each panel presents data from a different worm.

(A) Slow rhythmic undulations are evident posterior to the head.

(B) Rhythmic undulations in the mid-body arise after substantial damage is applied to the head.

(C) Rhythmic undulations in the neck and mid-body arise after substantial damage is applied to the head.

Figure S2. Related to Figure 3. Additional disruptions to motor coupling cause 2FU

(A) Two examples of worms in which all cholinergic neurons are inhibited (P*unc-17::NpHR*; global yellow illumination) except for those within a small tail region (P*unc-17::ChR2*; blue illumination in a small tail region). The A-type motor neurons were killed at the L2 larval stage (P*unc-4::MiniSOG*). Green triangle: worm head; blue band: blue illumination region. The curvature map (lower pane) indicates the spatiotemporal windows of yellow illumination (yellow dotted box) and blue laser illumination (white dotted box).

(B) 2FU induced by an inhomogeneous mechanical environment. Red dotted line indicates the boundary between low viscosity buffer (NGM) and high viscosity HPMC. Around t= 11s, the tail continues oscillating at high frequency even as the head rapidly slows to a crawl inside the HPMC.

Figure S3. Related to Figure 4. VNC premotor interneurons and several VNC motor neuron classes are not required for de-synchronized oscillations.

(A) 2FU occurs despite ablation of the premotor interneurons PVC (P*nmr-1::ICE*; P*myo-3::NpHR*). The spatiotemporal extent of green laser illumination is indicated by the white dotted box.

(B) 2FU occurs despite disruption of the gap junctions connecting AVB to the B-type motor neurons (*unc-7*; P*myo-3::NpHR*).

(C) 2FU occurs despite ablation of the A- and C-type motor neurons (P*unc-4::MiniSOG*; P*myo-3::NpHR*).

(D) When subjected to neck paralysis (P*myo-3::NpHR*), 2FU occurs reliably in P*nmr-1::ICE* and P*unc-4::MiniSOG* animals and occasionally in *unc-7* animals. Each colored circle pair represents one trial; worms may have multiple trials (see methods). N= 11, 8, and 16 worms per condition, respectively.

(E) Neck paralysis leads to modest decreases in tail bending amplitude in most conditions.

Figure S4. Related to Figure 4. Subsets of B-type motor neurons are not required for 2FU

Groups of 2-3 B-type motor neurons at a time were ablated using our pulsed infrared laser system in worms expressing P*myo-3::NpHR*; P*acr-2::RFP*. See also Figure 4F.

(A) Curvature maps of worms that exhibited 2FU despite ablation of the indicated B-type motor neurons and potentially some other neurons.

(B) RFP fluorescence images of each worm to confirm cell death. Blue labels indicate some or all B-type motor neurons. Red labels missing B-type neurons. White arrows indicate the vulva. All scale bars are 100 μm.

Figure S5. Related to Figure 4. B-type motor neurons posterior to the vulva are not required for 2FU

We attempted to ablate all B-type motor neurons posterior to the vulva in worms expressing P*myo-3::NpHR*; P*acr-2::RFP*.

(A) Curvature maps of worms that exhibited 2FU despite ablation of the indicated B-type motor neurons and potentially other neurons.

(B) RFP fluorescence images of each worm to confirm cell death. Blue labels indicate some or all B-type motor neurons. Red labels indicate missing B-type neurons. White arrows indicate the vulva. Scale bars:100 μm.

Figure S6. Related to Figure 5. Body undulations after severing the VNC and DNC do not require the A motor neurons

(A) Representative images of the VNC motor neurons in adult worms without (i) and with (ii) illumination with blue light at the L2 larval stage. After illumination, only B and AS neurons were visible along most of the body. In all worms tested however (N=20), at least one A motor neuron was visible at the posterior end of the VNC, corresponding to either VA12, DA8, or DA9. The behavior of the worm in (ii) is shown in C(i).

(B) Rhythmic waves visible posterior to the head after removal of the A motor neurons, severing the VNC and DNC in the neck, and damaging the head.

(C) Rhythmic waves visible in the mid-body (i) and tail (ii) after removal of the A motor neurons, severing the VNC and DNC in the neck, severing the VNC and DNC posterior to the vulva, and damaging the head.

Figure S7. Related to Figure 7. Rhythmic activity in the mid-body B motor neurons is sufficient for posterior-to-anterior entrainment, and muscle-to-muscle gap junctions are not required.

(A) Representative kymogram from a P*acr-5::Arch* worm that was subject to rhythmic (1.7 Hz) hyperpolarization of the mid-body B motor neurons (top), and average frequency spectra of the head before and during rhythmic inhibition (bottom). Note an increase in amplitude at 0.85Hz, one-half of the imposed frequency. N=22 trials were analyzed from 11 worms. Vertical red lines indicate the imposed mid-body frequency (solid) or one-half of the imposed frequency (dashed).

(B) Equivalent analysis for worms in which the mid-body muscles were rhythmically inhibited and muscle-to-muscle gap junctions are disrupted. Expression of UNC-9 in neurons was

transgenically restored (Wen et al., 2012). Note an increase in amplitude at 0.85 Hz, one half of the imposed frequency. N=22 trials were analyzed from 11 worms.

Figure S1 (Related to Figure 2). Tail undulation after gross head lesioning

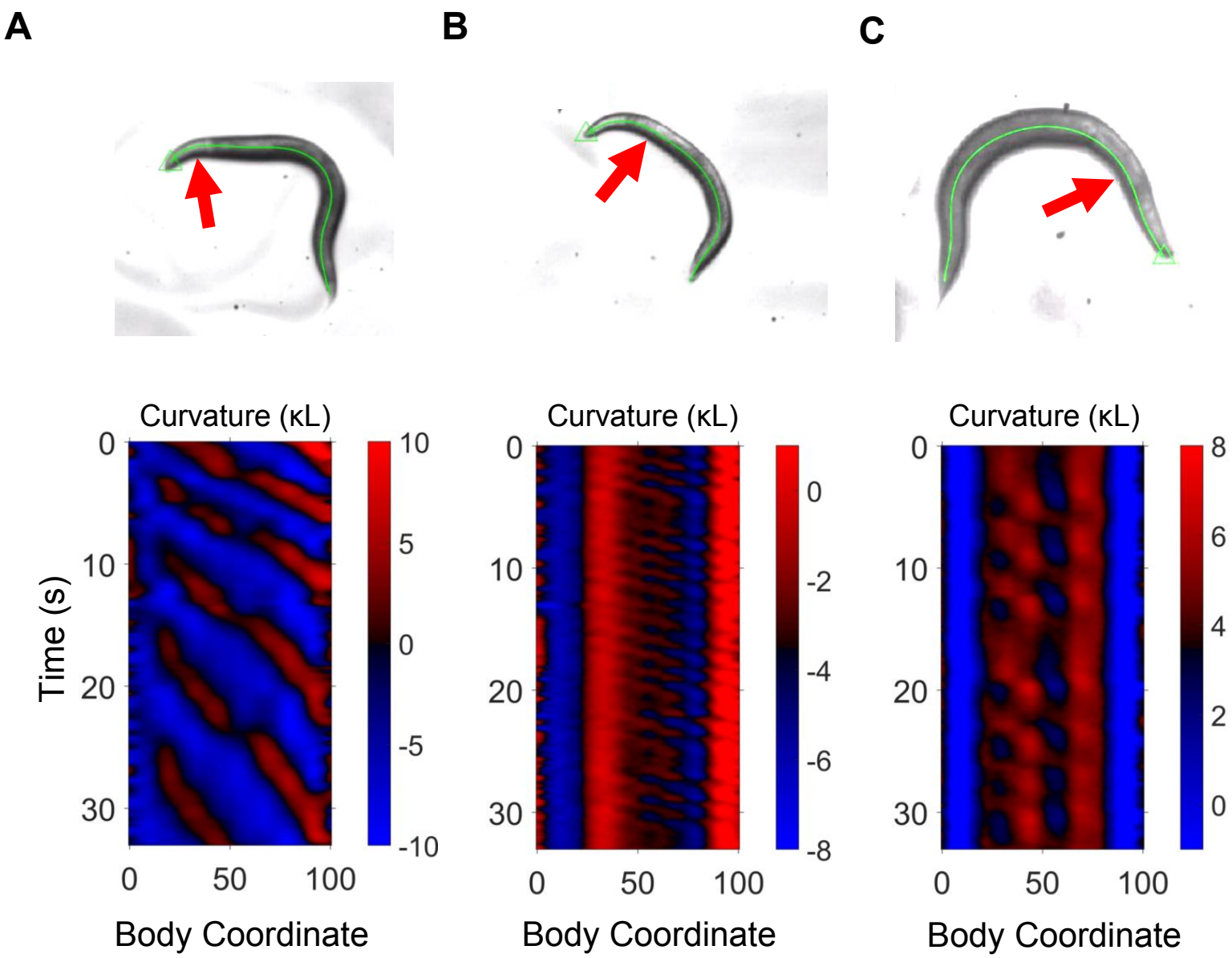

Supplemental Figure 1. Tail undulation after gross head lesioning. Red arrows indicate the approximate region lesioned.
a) Slow, rhythmic undulations are produced slightly posterior to the head, where the lesion occurred. b) Undulations primarily occurred in the midbody to tail region when the anterior third of the worm was lesioned. c) Slow undulations occurred in the middle of the body and quicker undulations in the tip of the tail were present when the head was lesioned.

Figure S2 (Related to Figure 3). Additional disruptions to motor coupling cause two-frequency undulation

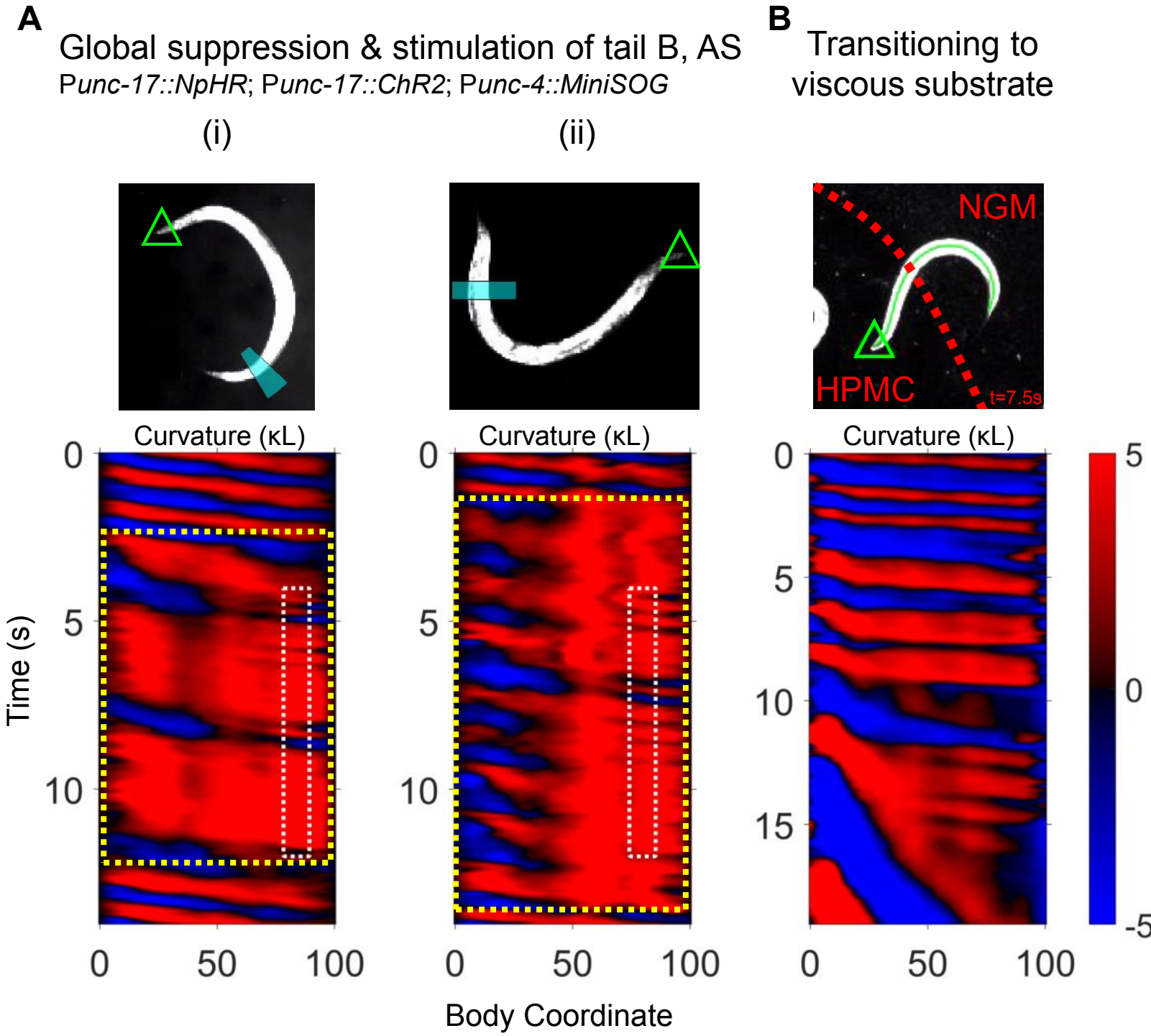

Figure S3 (Related to Figure 4). VNC premotor interneurons and several VNC motor neuron classes are not required for de-synchronized oscillations

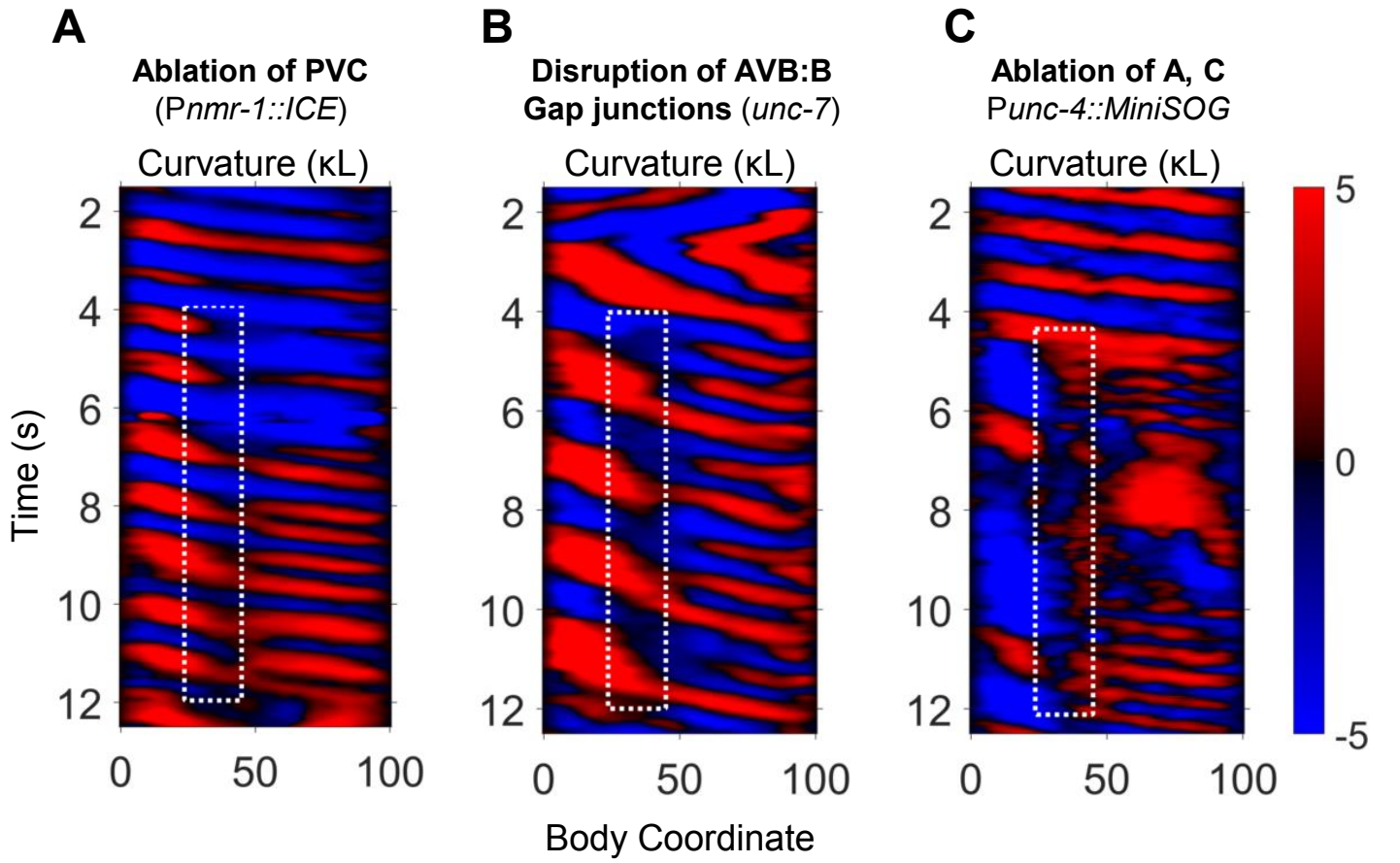

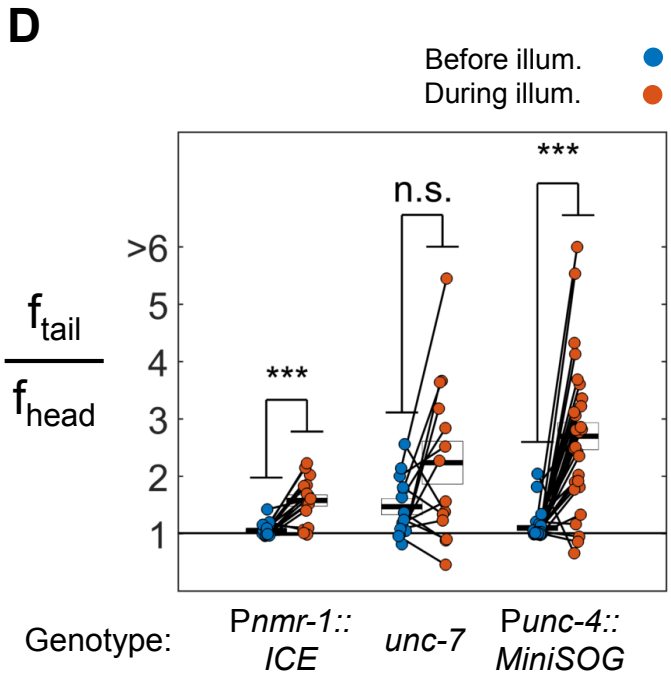

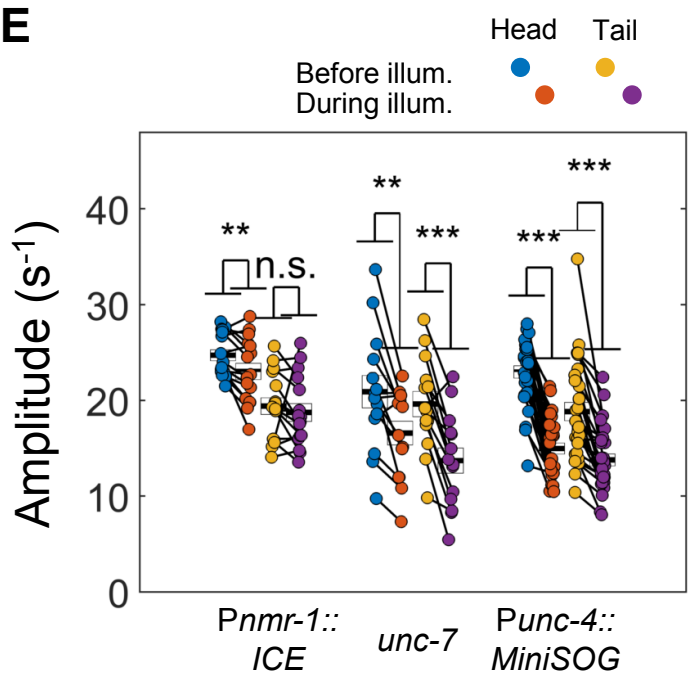

Figure S4 (Related to Figure 4). Subsets of B-type motor neurons are not required for 2FU

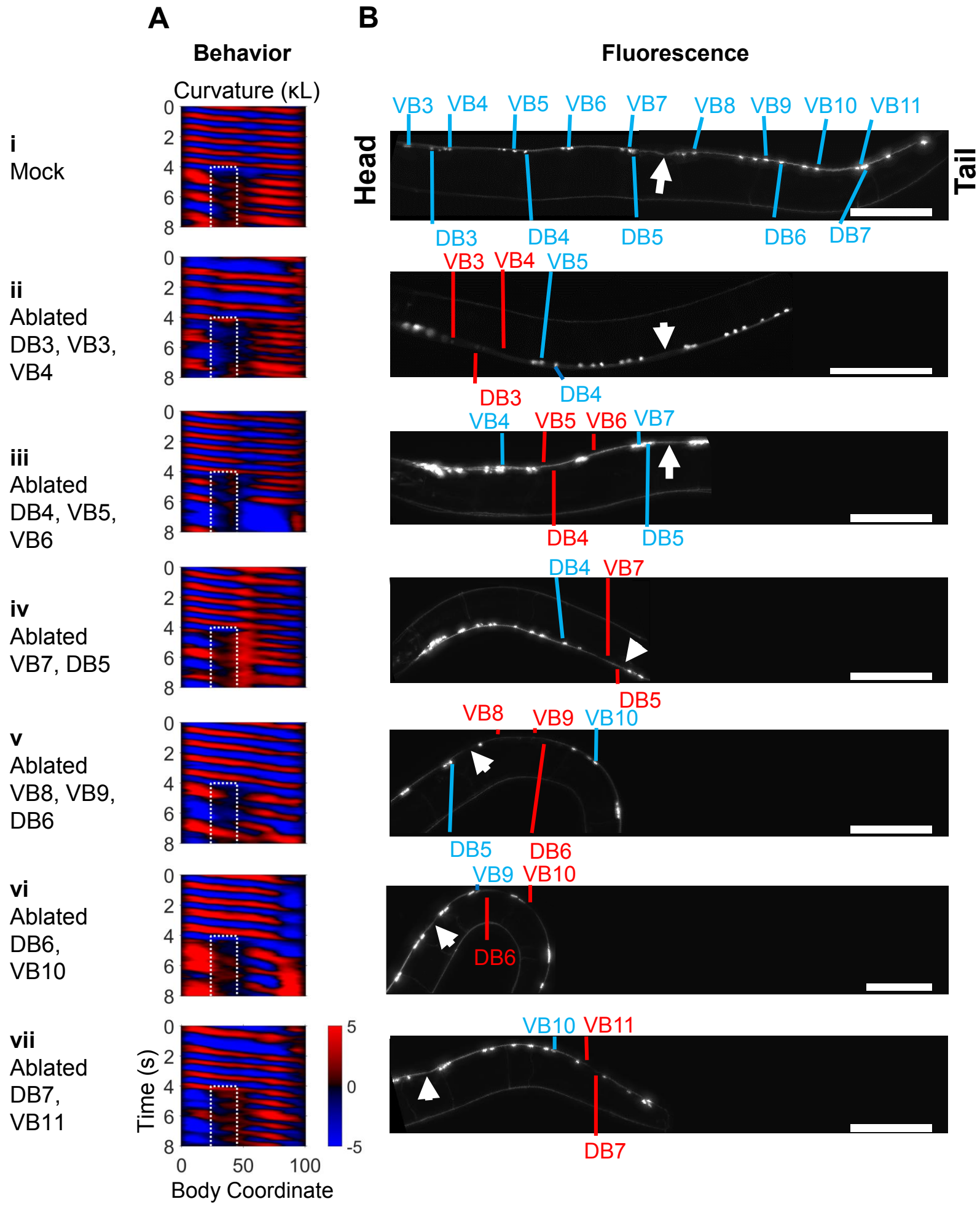

Figure S5 (Related to Figure 4). B-type motor neurons posterior to the vulva are not required for 2FU

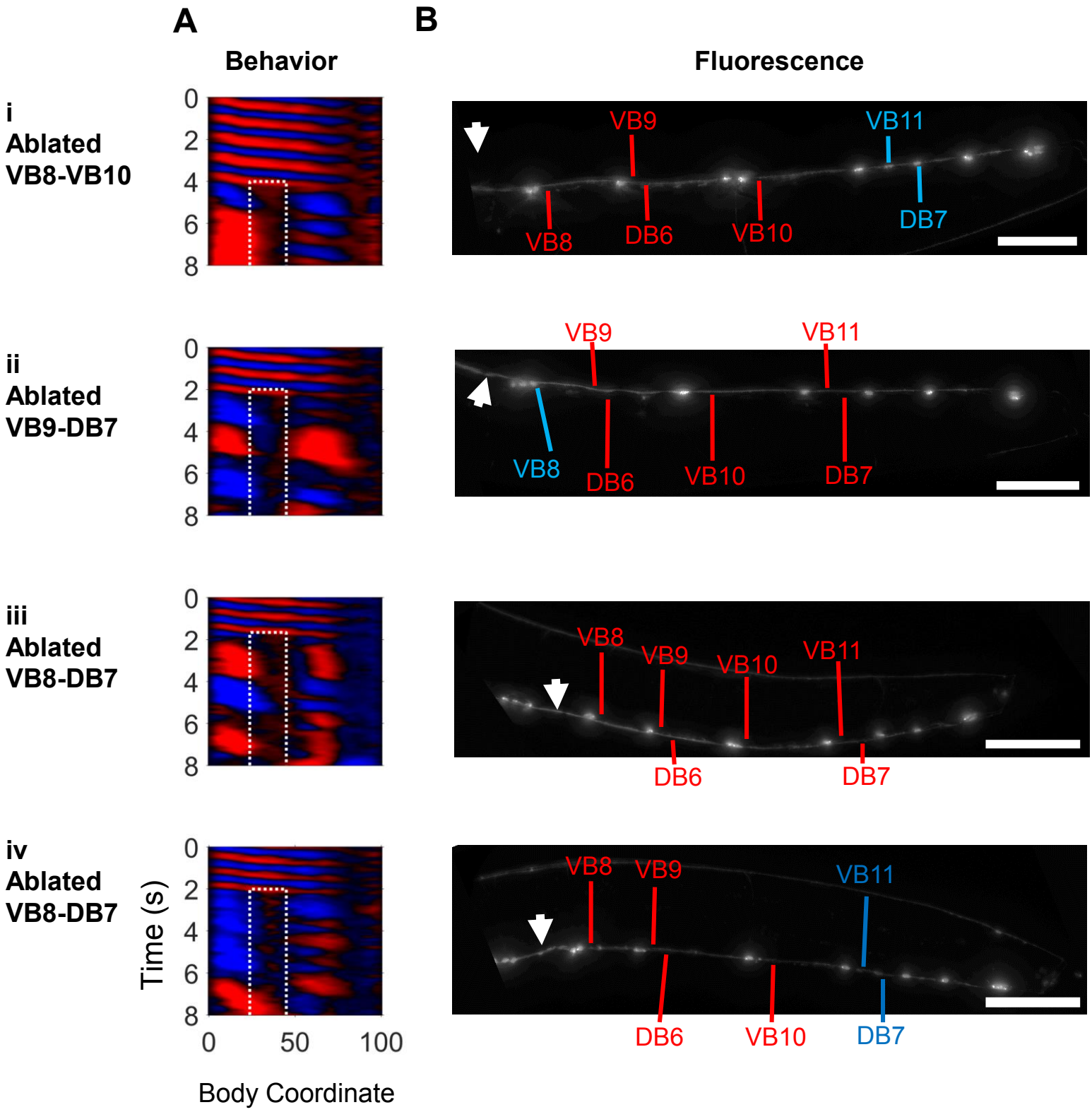

Figure S6 (Related to Figure 5). A motor neurons are not required for undulation after severing nerve cords

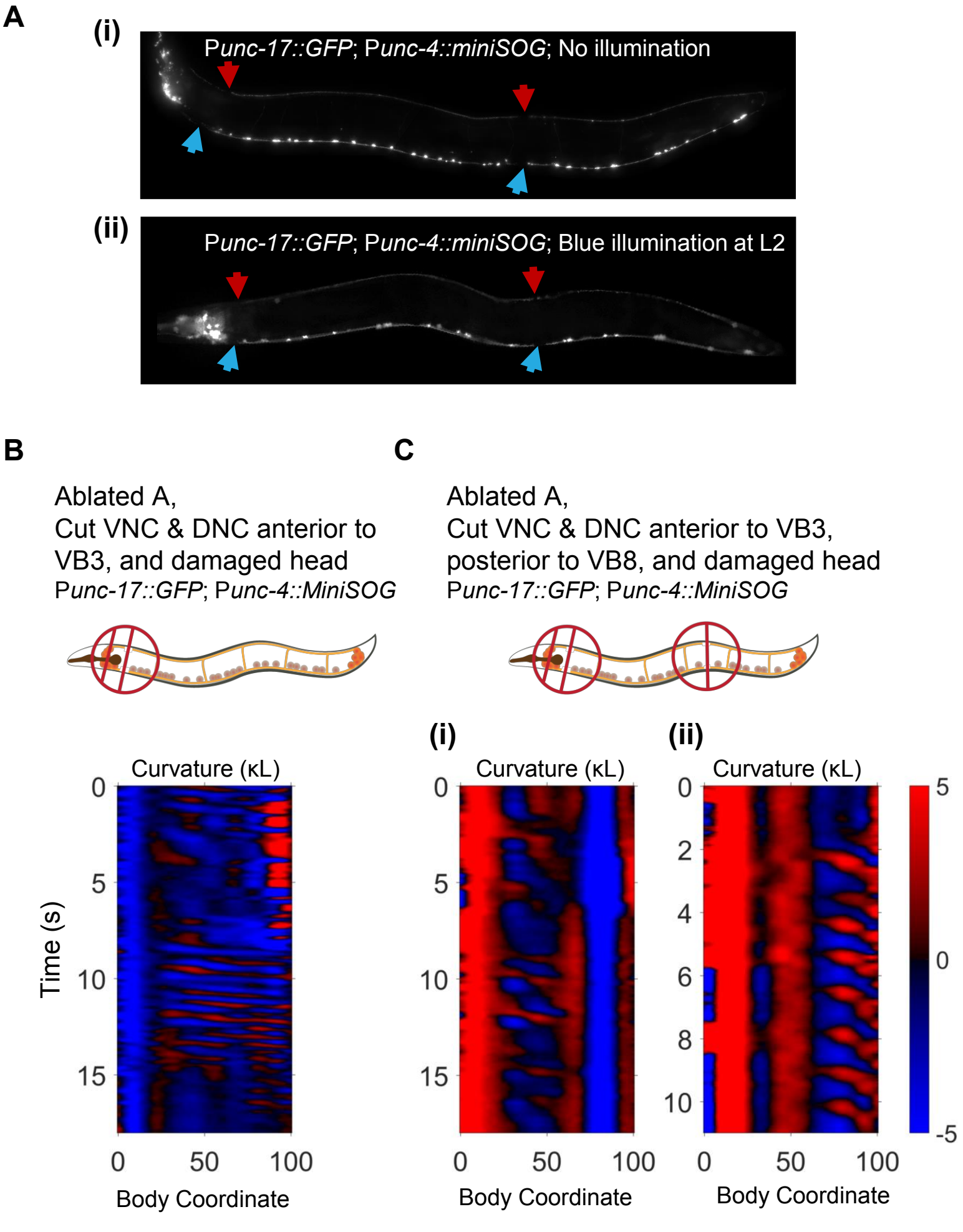

Figure S7 (Related to Figure 7). VNC Cholinergic neurons mediate posterior to anterior entrainment